



Universiteit  
Antwerpen

Faculteit Wetenschappen  
Department Wiskunde-Informatica

Estimation and removal of noise from single and  
multiple coil Magnetic Resonance images

---

Schatting en verwijdering van ruis in  
magnetische-resonantiebeelden opgemeten met  
één of meerdere spoelen

Proefschrift voorgelegd tot het belalen van de graad van  
**Doctor in de Wetenschappen**  
aan de Universiteit Antwerpen te verdedigen door  
**Jeny RAJAN**

Supervisor:

Prof. Dr. Jan Sijbers

Antwerpen, November 2012

---

## **Doctoral Committee**

### **Chairman**

Prof. Dr. Annie Cuyt

### **Members**

Prof. Dr. Jan Sijbers (Thesis supervisor)

Prof. Dr. Serge Demeyer

### **External members**

Prof. Dr. Frans Vos (Delft University of Technology)

Prof. Dr. Karel Deblaere (University of Ghent)

Copyright ©2012 by Jeny Rajan

This research work was financially supported by the Inter-University Attraction Poles Program 6-38 of the Belgian Science Policy, and by the SBO-project QUANTIVIAM (060819) of the Institute for the Promotion of Innovation through Science and Technology in Flanders (IWT-Vlaanderen), Belgium.

# Acknowledgment

I would like to thank all people who have helped and inspired me during my doctoral study.

My first debt of gratitude must go to my thesis advisor, Prof. Dr. Jan Sijbers. He helped me very much during my stay at the Vision lab, provided the proper guidance, encouragement and support throughout the doctoral study. Besides my advisor, I would like to thank the rest of my thesis jury members: Prof. Dr. Annie Cuyt, Prof. Dr. Serge Demeyer, Prof. Dr. Frans Vos and Prof. Dr. Karel Deblaere for the creative comments and suggestions.

My sincere thanks also goes to Prof. Dr. Marleen Verhoye, Johan Van Audekerke and Prof. Dr. Annemie Van der Linden of the Bio-Imaging lab for the collaboration, advice and help.

My special thanks to Luc Sanspoux, who provided me the accommodation in the initial days of my stay in Belgium.

I would like to acknowledge and extend my heartfelt gratitude to the professors and the past and present colleagues at the Vision Lab : Prof. Dr. Paul Scheunders, Prof. Dr. Joost Batenburg, Jaber Juntu, Jelle Veraart, Dr. Dirk Poot, Dr. Ben Jeurissen, Dr. Zenhua Mai , Maryna Kudzinava, Willem Jan Palenstijn, Dr. Wolfgang Jacquet, Zahid Mahmood, Hilde Segers, Gwendolyn Van Steenkiste, Dr. Toon Huysmans, Dr. Wim van Aarle, Dr. Guy Thoonen, Sander van der Maar, Dr. Romulo Pinho, Ruben Capiiau, Dr. Elke Van de Castele, Dr. Rob Heylen, Dr. Valérie De Witte, Muhammad Awais Akhter, Epameinondas Anastasiou, Dzevdet Burazerovic, Andrei Dabravolski, Joachim Ganseman, Jan-Pieter Jacobs, Tom Roelandts, Geert Van Eindhoven, Karim Zarei, Quinten Collier, Dr. Jan De Beenhouwer, Karen Dierckxsens, Tanmay Nath, Maarten Naeyaert...

Furthermore, thanks to Jose George, K. Kannan, Nissy Nevil, Dr. C. Kesavadas, Prof. Dr. M. R. Kaimal, Prof. Dr. K. Revathy, Prof. Dr. M. Wilscy, Madhu S Nair, S. Narayanan, Chandrasekhar P.S and Saji Raju for

---

their encouragement and moral support.

I owe my loving thanks to my wife Rani and to my daughter Nivedha. They have lost a lot due to my research abroad. Without their encouragement and understanding it would have been impossible for me to finish this work. My special gratitude is due to my mother, brother, sister and my in-laws for their loving support. Also, my loving thanks to my late father and grand parents.

Last but not least, thanks to God for giving me the determination and courage to overcome many trying moments to pursue my dreams.

Jeny Rajan

November 2012

# Contents

<b>List of Figures</b>	<b>ix</b>
<b>List of Tables</b>	<b>xiv</b>
<b>1 Introduction</b>	<b>1</b>
1.1 MR physics and imaging principles . . . . .	2
1.2 Noise in MRI . . . . .	6
1.3 Noise distribution in MRI . . . . .	8
1.4 Main contributions . . . . .	15
1.5 Thesis organization . . . . .	19
<b>2 Noise estimation from MR images</b>	<b>23</b>
2.1 Introduction . . . . .	24
2.2 Methods . . . . .	26
2.2.1 Noise estimation using local maximum likelihood estimation . . . . .	28
2.2.2 Noise estimation using measurement of local skewness . . . . .	29
2.3 Experimental Results . . . . .	33
2.4 Conclusion . . . . .	37
<b>3 Maximum likelihood estimation based denoising of MR Images</b>	<b>41</b>
3.1 Introduction . . . . .	42
3.2 Methods . . . . .	44
3.2.1 Signal estimation using LML . . . . .	44
3.2.2 Non local means algorithm . . . . .	45
3.2.3 Signal estimation using restricted LML . . . . .	47
3.2.4 Spatially varying noise levels . . . . .	48
3.3 Experiments and Results . . . . .	49
3.4 Conclusion . . . . .	57

<b>4 Estimation and removal of noise from multiple-coil MR images</b>	<b>67</b>
4.1 Introduction . . . . .	68
4.2 Theory . . . . .	69
4.3 Methods . . . . .	70
4.3.1 Extended NLML Method . . . . .	70
4.3.2 Estimation of the number of coils $L$ . . . . .	72
4.4 Experiments and Results . . . . .	74
4.5 Conclusion . . . . .	79
<b>Conclusions</b>	<b>85</b>
<b>List of Publications</b>	<b>87</b>

# Samenvatting

Het schatten en reduceren van ruis uit Magnetische Resonantie (MR) beelden is belangrijk voor interpretatie, analyse, accurate parameterschatting en verdere verwerking van deze beelden. Ruis blijft één van de belangrijkste oorzaken van kwaliteitsvermindering in MRI en maakte reeds het onderwerp uit van diverse papers in de MRI literatuur. Deze thesis omvat de beschrijving van nieuwe methoden voor het schatten van ruis en voor het reduceren van ruis in MRI beelden die zowel met enkelvoudige als met meervoudige spoelen werden opgenomen. De belangrijkste bijdragen in deze thesis kunnen als volgt worden samengevat: (i) Schatting van ruis uit MRI beelden in afwezigheid van achtergrond signaal (ii) Effectieve ruisreductie van MRI beelden en (iii) Methoden voor de schatting en reductie van ruis in MR beelden opgenomen bij meervoudige spoelen.

De meeste van eerder voorgestelde methoden voor ruisreductie zijn gestoeld op de Rayleigh verdeelde achtergrondgebieden in magnitude MRI beelden. Deze methoden kunnen vanzelfsprekend niet gebruikt worden indien weinig of geen achtergrond signaal aanwezig is. In deze thesis stellen we twee verschillende object gebaseerde methoden voor, voor de schatting van het ruisniveau vanuit Rice verdeelde magnitude MR data, welke geen gebruik maken van achtergrond data. De eerste methode is gebaseerd op de lokale schatting van de ruisvariantie via maximum likelihood schatting; de tweede methode is gebaseerd op de lokale schatting van de scheefheid van de magnitude MR data distributie.

Voor de reductie van ruis in MRI beelden, wordt een maximum likelihood schattingsmethode voorgesteld die gebaseerd is op gerestricteerde, lokale omgevingen. De conventionele maximum likelihood methoden voor het schatten van het onderliggende signaal, baseerden zich op de Rice verdeling, waarbij het signaal constant of traagvariërend werd verondersteld in een lokaal gebiedje. Indien deze aanname niet geldig is, leidt dergelijke filtering

echter tot wazige randen en verlies van kleine details. Om hiervoor een oplossing te bieden wordt het concept van gerestricteerde lokale omgevingen voorgesteld waar het ruisloze, onderliggende signaal wordt geschat voor elke pixel vanuit een set van voorgeselecteerde omgevingspixels. Daartoe wordt eerst een referentiebeeld gecreëerd van het ruizige beeld uitgaande van een recent voorgesteld niet-lokale-gemiddelden algoritme. Dit referentiebeeld wordt gebruikt als voorkennis voor verdere ruisreductie.

Hoewel in de literatuur veel methoden werden voorgesteld voor het schatten en reduceren van ruis, werden slechts weinig algoritmen beschreven voor de schatting van ruis en het onderliggend signaal uit MR beelden die werden opgenomen met multi-kanaals-oppervlaktespoelen. Dergelijke meervoudige spoelen worden hoe langer hoe meer gebruikt in de praktijk. Meervoudige opnamespoelen werden aanvankelijk ontwikkeld om de signaal-ruis-verhouding (SNR) van de op te nemen beelden te verbeteren. In een later stadium werden parallelle MRI (pMRI) technieken ontwikkeld om het MRI opnameschema te versnellen via onderbemonstering van de  $k$ -ruimte. Echter, parallelle beeldvormings- en reconstructiemethoden kunnen de statistische eigenschappen veranderen van de data in het gereconstrueerde beeld. De onderbemonstering van de  $k$ -ruimte resulteert in een spatiaal variërend ruisniveau. In deze thesis worden methoden voorgesteld voor het schatten van het ruisniveau en onderliggend signaal van MR beelden afkomstig van multi-opnamespoel-systemen, waarbij de gereconstrueerde data een niet-centrale  $\chi$ -verdeling volgt.

# Summary

Estimation and removal of noise from Magnetic Resonance (MR) images is important for proper interpretation, analysis, accurate parameter estimation and for further preprocessing of these images. Noise remains one of the main causes of quality deterioration in MRI and is a subject in a large number of papers in the MRI literature. This thesis aims to provide new approaches for noise estimation and noise removal from both single and multiple coil acquired magnitude MR images. The main contributions in this thesis can be summarized as: (i) Estimation of noise from MRI in the absence of a background region (ii) Effective denoising of MRI and (iii) Methods for noise estimation and denoising of multiple-coil acquired MR images.

For noise estimation, most of the methods proposed earlier exploited the Rayleigh distributed background region in the magnitude MR images. These methods, however, cannot be used for images in which no background information is available. In this thesis, we propose two different object based approaches for noise level estimation from Rician distributed magnitude MR data. These methods don't rely on the image background. The first method is based on the local estimation of the noise variance using maximum likelihood estimation and the second method is based on the local estimation of the skewness of the magnitude data distribution.

For the denoising of MRI, we propose a maximum likelihood estimation method using restricted local neighborhoods. Conventionally, maximum likelihood methods incorporate the Rice distribution to estimate the true underlying signal from a local neighborhood within which the signal is assumed to be constant. However, if this assumption is not met, such filtering will lead to blurred edges and loss of fine structures. As a solution to this problem, we put forward the concept of restricted local neighborhoods where the true intensity for each noisy pixel is estimated from a set of preselected neighboring pixels. To this end, a reference image is created from the noisy

image using a recently proposed non local means algorithm. This reference image is used as a prior for further noise reduction. A scheme is developed to locally select an appropriate subset of pixels from which the underlying signal is estimated.

Even though many methods were proposed in the literature for MRI noise estimation and denoising, not many approaches were suggested for estimating noise or underlying true signal from MR images acquired with multichannel surface-coil arrays. Nowadays, multiple coil MRIs are becoming more common. Multiple coil systems were initially developed to enhance the signal to noise ratio (SNR) of the acquired images and later parallel MRI (pMRI) techniques were employed to it, to accelerate the acquisition process through  $k$ -space subsampling. However, parallel imaging and reconstruction methods can influence the statistical distribution of the data. The subsampling of  $k$ -space makes the noise level in the image spatially varying. In this thesis we propose methods for estimating the noise level and underlying true signal from multiple-coil acquired MR images in which the data follows a non central- $\chi$  distribution.

# List of Figures

1.1	MR image of a Kiwi fruit (a) and (b) $k$ -space images (c) and (d) real and imaginary parts of the complex image after inverse Fourier transform (e) magnitude image (f) phase image. . . . .	7
1.2	Rician PDF for different SNR values. . . . .	10
1.3	Histogram of the background region of the Kiwi fruit in Fig.1.1 (a) histogram of the real part (b) histogram of the imaginary part (c) histogram of the magnitude image. . . . .	11
1.4	Distribution of pixels in different regions of a simulated noisy MR image (a) simulated noisy MR images with noise level $\sigma_g = 30$ , (b) distribution of pixels in the background region (c) distribution of pixels in the CSF region (d) distribution of pixels in the grey matter region (e) distribution of pixels in the white matter region. . . . .	12
1.5	nc- $\chi$ PDF for different values of L. . . . .	15
1.6	Issues with histogram based methods for noise estimation (a) and (b) noisy images with a noise level of $\sigma_g = 20$ and $\sigma_g = 60$ respectively (c) and (d) corresponding histograms. . . . .	18
1.7	Images with artifacts in the background region . . . . .	18
1.8	Rician Bias : This experiment was conducted with $\sigma_g = 1$ and varying $a$ from 0.5 to 20 . . . . .	19
2.1	Background segmentation from MR images (a) and (c) noisy MR images with Rayleigh background (b) and (d) segmented background regions. . . . .	27
2.2	Relation between the SNR and skewness for Rician distributed data . . . . .	31
2.3	Relation between the SNR and correction factor for Rician distributed data . . . . .	31
2.4	Relation between the skewness and variance correction factor for Rician distributed data . . . . .	32

2.5	Noisy MR images of the brain (a) and heart (b), both corrupted with Rician noise with $\sigma_g = 50$ . On the right, the distribution of local estimates of $\sigma_g$ computed using both ML (solid red line) and skewness based methods (dashed blue line) are shown for both the brain (c) and the cardiac (d) images. . . . .	34
2.6	The estimated $\sigma_g$ / actual $\sigma_g$ for various values of $\sigma_g$ ranging from 10 to 100. This experiment was done on the Cardiac MR image. The red and blue line corresponds to the proposed methods using ML and skewness, respectively, and the green line corresponds to the estimator given in Eq. (2.3). The shaded area shows the standard deviation for 100 experiments. . . . .	35
2.7	Elapsed time for noise estimation with ML and skewness based methods for image size varying from $50 \times 50$ to $300 \times 300$ . . . . .	35
2.8	Precision and accuracy of the proposed ML based estimator for different window size. . . . .	36
2.9	Precision and accuracy of the proposed skewness based estimator for different window size. . . . .	36
2.10	MR images of cherry tomato (a) acquired without averaging (b)acquired with 6 averages (c) acquired with 12 averages. . . . .	36
2.11	Estimated $\sigma_g$ as a function of the number of averages $n$ used during the acquisition. MR image of a cherry tomato was used for this experiment. . . . .	37
3.1	Denoising MRI with LML method (a) Original image (b) Original image corrupted with Rician noise of $\sigma_g = 15$ . (c) Noisy image denoised with LML of window size $3 \times 3 \times 3$ (d) Noisy image denoised with LML of window size $5 \times 5 \times 3$ . The blurring effect generated by the LML method can be observed from the denoised images. . . . .	46

3.2	Computation of threshold from ROI and from the mode of the local distribution of range (a) Reference image with ROI (marked as red) (b) distribution of intensity in the ROI (c) distribution of local range computed using $3 \times 3$ and $5 \times 5$ neighborhood. . . . .	48
3.3	Denoising MRI with various methods : (a) Original image (b) Original image corrupted with Rician noise of $\sigma_g = 20$ (c) (b) denoised with NLML method (d) (b) denoised with UNLM method (e) (b) denoised with RNRAD method (f) (b) denoised with RLML method (g), (h), (i), (j) are the residual images (in the range 0 - 25) of (c), (d), (e), (f). . . . .	52
3.4	Comparison of the histograms of the simulated ground truth (GT) with the histogram of the denoised images (a) with NLML (b) with UNLM (c) with RNRAD (d) with RLML. . . . .	53
3.5	Quantitative analysis of the proposed method with other recently proposed methods based on (a) PSNR (b) SSIM (c) BC and (d) MAD for image corrupted with Rician noise of $\sigma_g$ varying from 5 to 80. . . . .	54
3.6	Denoising MRI with spatially varying noise levels (a) Noisy image with spatially varying noise (b) noise modulation map (c) noisy image denoised with ARNLM method (d) noisy image denoised with proposed RLML method. . . . .	55
3.7	Denoising SENSE reconstructed MRI with 4 coils and acceleration factor = 2 (a) Noisy image with spatially varying noise (b) with ARNLM (PSNR : 31.1639 (c) with RLML using Eq. (3.9) PSNR : 31.7544 . . . . .	55
3.8	Performance comparison of the RLML method against a recently proposed ARNLM method in terms of (a) PSNR (b) SSIM (c) BC and (d) MAD for image corrupted with spatially varying Rician noise of $\sigma_g$ varying from 5 to 80. . . . .	56

3.9	Experiments on the DWI atlas of the human brain (a) FA map computed from the ground truth (b) FA map computed after corrupting the original image with Rician noise of $\sigma_g = 100$ (c) FA map computed from the image denoised with NLML method (d) FA map computed from the image denoised with UNLM method (e) FA map computed from the image denoised with RNRAD method (d) FA map computed from the image denoised with the proposed RLML method. . . . .	58
3.10	Absolute FA residuals (a) Noisy (MAD : 0.1189) (b) NLML method (MAD : 0.0560) (c) UNLM method (MAD : 0.0531) (d) RNRAD method (MAD : 0.0640) (e) proposed RLML method (MAD : 0.0505). . . . .	59
3.11	Experiments on the MR image of a Kiwi fruit <b>(a)</b> Original image reconstructed with 1 average <b>(b)</b> Original image reconstructed with 12 averages <b>(c)</b> (a) denoised with NLML method (sample size :18) <b>(d)</b> (a) denoised with UNLM method <b>(e)</b> (a) denoised with RNRAD method <b>(f)</b> (a) denoised with RLML method. . . . .	60
4.1	Denoising of MRI with $nc-\chi$ distributed noise. (a) Ground Truth reconstructed with SoS method with $L = 8$ (b) Ground Truth corrupted with $nc-\chi$ distributed noise of $\sigma_g = 15$ (c) denoised with LMMSE method (d) denoised with proposed method (e) and (f) corresponding residual images of (c) and (d) (scale 0-25). . . . .	76

4.2	Denoising of multiple-coil acquired MRI. (a)[PSNR: 29.49,MSSIM: 0.8256], (b)[PSNR: 24.44,MSSIM: 0.6749] and (c)[PSNR: 24.77,MSSIM: 0.6848] are images acquired with $L = 4$ and $\sigma_g = 10$ and reconstructed with SoS, SENSE and GRAPPA (acceleration factor: 2) respectively. (d) [PSNR: 34.88, MSSIM: 0.9714], (e) [PSNR: 31.81, MSSIM: 0.9079] and (f) [PSNR: 28.41, MSSIM : 0.9111] are the denoised images of SoS, SENSE and GRAPPA reconstructed images. (g),(h) and (i) are the corresponding residual images (scale 0-25) with respect to the Ground Truth . . . . .	78
4.3	Experiments on ex vivo mice images. (a) (b) and (c) original mice image acquired with $2 \times 2$ channel phased array coil and reconstructed with SoS, SENSE and GRAPPA. (d), (e) and (f) are the corresponding denoised images using the proposed method. . . . .	79
4.4	Actual distribution of the background region of the mice image (acquired with SoS with $L = 4$ ) compared with the central- $\chi$ PDF (with $L = 4$ and $\sigma_g$ estimated from the background region of the image). . . . .	80

# List of Tables

2.1	Values of the coefficients in Eq. (2.17) . . . . .	32
3.1	Quantitative analysis of the proposed method with other recently proposed methods based on Eq. (3.11). This experiment was conducted on the MR image of a kiwi fruit. . . . .	61
4.1	<i>SNR</i> of the central $\chi$ distributed background region for different values of $L$ . . . . .	74
4.2	Quantitative analysis of the proposed method with LMMSE method proposed in [10]. This experiment was conducted on the synthetic image of the brain reconstructed with SoS method with $L = 8$ . . . . .	75

# Introduction

---

## Contents

---

<b>1.1 MR physics and imaging principles . . . . .</b>	<b>2</b>
<b>1.2 Noise in MRI . . . . .</b>	<b>6</b>
<b>1.3 Noise distribution in MRI . . . . .</b>	<b>8</b>
<b>1.4 Main contributions . . . . .</b>	<b>15</b>
<b>1.5 Thesis organization . . . . .</b>	<b>19</b>

---

Magnetic Resonance Imaging (MRI) is based on the phenomenon of nuclear magnetic resonance (NMR or MR), which was first described and measured by Isidor Rabi [1] and later the technique was expanded by Felix Bloch [2, 3] and Edward Purcell [4]. For their discovery of NMR, Rabi was awarded the Nobel price in physics in 1944 and Bloch and Purcell shared the Nobel price in Physics in 1952. The potential of NMR spectroscopy was recognized almost immediately after its discovery and was used for chemical and physical molecular analysis. Later this wonderful phenomenon was exploited for imaging for which the MRI community mainly owes to the pioneering work of Raymond Damadian [5], Paul Lauterbur [6], Anil Kumar and Richard Ernst [7] and Peter Mansfield [8]. Despite its relatively slow beginning, MRI has become an indispensable diagnostic tool and an important noninvasive imaging modality since the early 1980s. MRI has found a number of applications in the fields of biology, engineering, and material science. Because it provides unique contrast between soft tissues and high spatial resolution, MRI has revolutionized

diagnostic imaging in medical science [9]. An important advantage of diagnostic MRI as compared to CT is that the former does not use ionizing radiation since MRI operates in the radio frequency (RF) range.

In this chapter, the principles of MRI are introduced first, followed by the source of noise in MRI and its statistics. Finally, the main contributions of this thesis are summarized and the structure of the thesis is explained.

### 1.1 MR physics and imaging principles

A brief introduction to MRI is given in this section. For a deeper study of MRI physical principles, it is referred to the works in [10, 11, 9]; part of the material of this section has been extracted from these texts.

NMR is based upon the interaction between an applied magnetic field and a nucleus that possesses spin. Nuclear spin or nuclear spin angular momentum is one of several intrinsic properties of an atom and its value depends on the precise atomic composition [10]. A nucleus with a spin quantum number,  $I=0$ , does not interact with an external magnetic field and cannot be studied using NMR. The  $^1\text{H}$  nucleus, consisting of a single proton with a spin of  $1/2$ , is the most commonly used MR active nuclei for probing the human body and is primarily because of two reasons. (i)  $^1\text{H}$  is by far the most abundant in the body (mainly in  $\text{H}_2\text{O}$ ) (ii) its response to an applied magnetic field is one of the largest found in the nature [10, 11].

In addition to its spin, a charged nucleus also has a local magnetic moment ( $\vec{\mu}$ ) given by

$$\vec{\mu} = \gamma \vec{p} \quad (1.1)$$

where  $\vec{p}$  is the spin angular momentum of the nucleus and  $\gamma$  is a constant for each nucleus, known as gyromagnetic ratio. The collective behavior of the spin system can be represented using a macroscopic magnetization vector  $\vec{M}$ , which is the vector sum of all the microscopic magnetic moments in the object:

$$\vec{M} = \sum_{i=1}^{N_s} \vec{\mu}_i \quad (1.2)$$

---

### 1.1. MR physics and imaging principles

where  $\vec{\mu}_i$  is the magnetic moment of the  $i^{\text{th}}$  nuclear spin and  $N_s$  is the total number of spins. In the absence of an external magnetic field, the spins are oriented randomly, and as a result the net magnetization  $\vec{M}$  will be zero. However, when placed in a magnetic field of strength  $\vec{B}_0$ , two notable effects occur. First, the  $\vec{B}_0$  field polarizes the sample, inducing a net magnetization moment  $\vec{M}_0$  in the  $z$ -direction. By convention, the direction of the applied field is called the  $z$ -direction or *longitudinal* direction. Second, the nucleus will precess at a frequency  $\omega_0$ . This precessional frequency is proportional to the strength of the magnetic field and is called the Larmor frequency. The relationship between  $\omega_0$  and  $\vec{B}_0$  is given in the Larmor equation as:

$$\omega_0 = \gamma B_0 \quad (1.3)$$

The magnetization  $M_0$  per unit volume is given by:

$$M_0 = \frac{n_I \hbar^2 \gamma^2 I(I+1)}{3kT} B_0 \quad (1.4)$$

where  $n_I$  is the number of nuclear spins per unit volume,  $\hbar$  is the reduced Planck's constant,  $k$  is Boltzmann's constant and  $T$  is the absolute temperature. This induced magnetization,  $M_0$ , is the source of signal for all the MR experiments.

To obtain an MR signal, an RF magnetic pulse  $\vec{B}_1$  tuned to the Larmor frequency of the spins is applied in the  $xy$  (transverse) plane to excite the spins out of equilibrium state. Effectively,  $\vec{B}_1$  applies a torque which rotates the magnetization vectors by a prescribed angle dependent on the strength of  $\vec{B}_1$  and its duration. If the excitation is set for a  $90^\circ$  tip angle, then upon turning the excitation off, the tipped vectors precess in the  $xy$  plane at the Larmor frequency. After excitation, the net magnetization  $\vec{M}$  relaxes back to its original state. The time constant characterizing the return of the magnetization vector along the  $z$ -axis (longitudinal axis) is called  $T_1$  (spin-lattice relaxation time), while the time constant characterizing the decay of the vector component in the  $xy$  plane (transverse plane) is called  $T_2$  (spin-spin relaxation time). The dynamics of  $\vec{M}$  due to excitation and relaxation are phenomenologically described by the *Bloch* equations [3]:

$$\frac{d}{dt} M_x(t) = \gamma M_y B_0 - \frac{M_x}{T_2} \quad (1.5)$$

---

### 1.1. MR physics and imaging principles

$$\frac{d}{dt}M_y(t) = -\gamma M_x B_0 - \frac{M_y}{T_2} \quad (1.6)$$

$$\frac{d}{dt}M_z(t) = -\frac{M_z - M_0}{T_1} \quad (1.7)$$

where  $M_x$ ,  $M_y$  and  $M_z$  are the components of  $\vec{M}$  along  $x$ ,  $y$ , and  $z$  directions. The solutions to the differential equations in Equations (1.5), (1.6) and (1.7) are [9]:

$$M_x(t) = [M_x(0) \cos(\omega_0 t) + M_y(0) \sin(\omega_0 t)] \exp(-t/T_2) \quad (1.8)$$

$$M_y(t) = [-M_x(0) \sin(\omega_0 t) + M_y(0) \cos(\omega_0 t)] \exp(-t/T_2) \quad (1.9)$$

$$M_z(t) = M_0 + [M_z(0) - M_0] \exp(-t/T_1) \quad (1.10)$$

where  $M_x(0)$ ,  $M_y(0)$  and  $M_z(0)$  are the initial values of  $M_x$ ,  $M_y$  and  $M_z$ . By defining the transverse magnetization,  $M_{xy}$ , as  $M_{xy} = M_x(t) + iM_y(t)$ , where  $i = \sqrt{-1}$ , we can write:

$$M_{xy}(t) = M_0 e^{-t/T_2} e^{i\omega_0 t} \quad (1.11)$$

and

$$M_z(t) = M_0(1 - e^{-t/T_1}) \quad (1.12)$$

where  $M_{xy}(0) = 1$  and  $M_z(0) = 0$ . The precessional frequency  $\omega_0$  is typically demodulated out of the transverse magnetization to obtain:

$$M_{xy}(t) = M_0 e^{-t/T_2} \quad (1.13)$$

From Faraday's law of induction, the rotating magnetization vectors induce an electromotive force (EMF) in an RF receiver coil oriented to detect changes in the magnetization in the  $xy$  plane. The generated time signal is called free induction decay (FID). In general, a set of FIDs will be recorded and precessed to reconstruct and MR image.

If the applied field is only the main static field  $\vec{B}_0$  in the  $z$ -direction, then all spins possess the same resonance frequency and if excited, behave like oscillators inducing signals at that frequency. Because the excitation/receiver RF coil encompasses the entire region of interest, it is not possible to excite a selected portion of the volume nor is it possible to distinguish the signals generated from different spatial location if only  $B_0$  exists. Introducing magnetic

---

### 1.1. MR physics and imaging principles

field gradients allow spatial information to be obtained from analysis of the MR signal. This gradient can be expressed as a vector  $\vec{G} = G_x\hat{i} + G_y\hat{j} + G_z\hat{k}$ , where  $G_z$  is the slice selection gradient,  $G_x$ , the frequency encoding and  $G_y$ , the phase encoding. In the presence of Gradient  $\vec{G}$ , the magnetic field  $\vec{B}$  can be written as:

$$\vec{B}(\vec{r}) = (B_0 + \vec{G} \cdot \vec{r})\hat{k} \quad (1.14)$$

where  $\vec{r} = x\hat{i} + y\hat{j} + z\hat{k}$ . The presence of magnetic field gradients requires an expanded version of the Larmor and can be written as:

$$\omega(\vec{r}) = \gamma(B_0 + \vec{G} \cdot \vec{r}) \quad (1.15)$$

where  $\omega(\vec{r})$  is the frequency of the proton at  $\vec{r}$ . The above equation states that, in the presence of a gradient field, each proton will resonate at a unique frequency that depends on its exact position within the gradient field. The MR image is simply a frequency and phase map of the protons generated by unique magnetic fields at each point throughout the image. After, frequency and phase encoding, the signal in the  $k$ -space for a particular slice can be written as

$$s(k_x, k_y) = \int_x \int_y M_{xy}(x, y) e^{-i(xk_x + yk_y)} dx dy \quad (1.16)$$

where

$$k_x = \gamma \int_0^t G_x dt \quad (1.17)$$

and

$$k_y = \gamma \int_0^t G_y dt \quad (1.18)$$

Eq. (1.16) shows that the data matrix  $s(k_x, k_y)$  is a sampling of the Fourier coefficients of the function  $M_{xy}(x, y)$ . Therefore, by applying a two-dimensional inverse Fourier transform to the  $k$ -space data  $s(k_x, k_y)$ , the result will be an estimate of the function  $M_{xy}(x, y)$ . Because of quadrature detection, there will be two  $k$ -space images with  $90^\circ$  phase difference and these two data streams are usually represented as real and imaginary parts of the “complex” MR signal. Inverse Fourier transform of the complex  $k$ -space will generate a complex image. Magnitude and phase images are then created from the complex MR

image. Although all information is in the complex images, it is common practice to work with magnitude and phase images instead as they have more physical meaning (proton density, flow, etc) [12]. Fig. 1.1 shows the MR image of a kiwi fruit at various stages, i.e. from  $k$ -space to magnitude image.

## 1.2 Noise in MRI

The principal source of noise in MRI is thermal in origin which is produced by the stochastic motion of free electrons. These free electrons collide with atoms, resulting in an exchange of energy and generates random electrical fluctuations. The source of noise in MRI are these randomly fluctuating currents in the sample (imaged object) and in the receiver coil. The resulting noise power given by the Johnson formula [9] is:

$$\langle V^2 \rangle = 4kT(R_{coil} + R_{body}) \quad (1.19)$$

where  $V^2$  is the noise power,  $k$  is the Boltzmann's constant,  $T$  is the absolute temperature (in Kelvin) and  $R_{coil}$  and  $R_{body}$  are the effective resistances in the receiver coil and the sample respectively. Thus the total noise power within a bandwidth  $\Delta f$  is  $4kT(R_{coil} + R_{body})\Delta f$ . The thermal noise is considered to be white, additive and follows a Gaussian distribution with a variance  $\sigma_g^2$  and mean zero. A formula for calculating the effective resistance of the sample is derived in [13]. Often, the dominant source of noise is from the body and not from the receiver coil. The body, being a conductive medium, generates fluctuating fields that will be picked up by the receiver coil. However, in certain cases, such as low-field imaging and small-volume imaging, the resistance inherent to the receiver coil will represent the dominant source of noise [11]. An additional noise source is from the pre-amplifier through which the signal from the coil is passed.

The noise variance is also influenced by the imaging parameters. These parameters include the number of samples in the  $x$  and  $y$  directions ( $N_x$ ,  $N_y$ ), the number of averages ( $n$ ), the field of view in the  $x$  and  $y$  directions ( $w_x$ ,  $w_y$ ) and the sampling interval ( $\Delta t$ ). The relationship of these parameters to

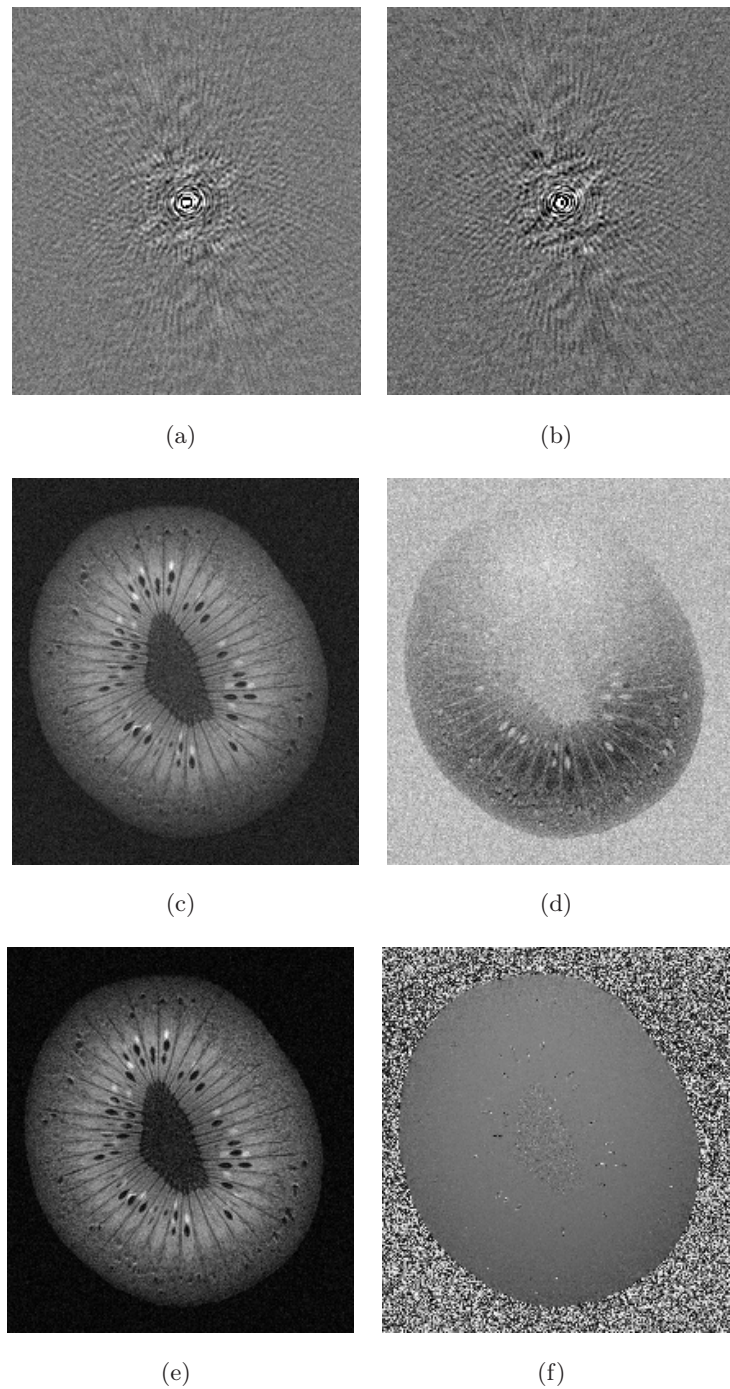


Figure 1.1: MR image of a Kiwi fruit (a) and (b)  $k$ -space images (c) and (d) real and imaginary parts of the complex image after inverse Fourier transform (e) magnitude image (f) phase image.

the image noise variance was discussed in detail by Parker and Gullberg [14] and is given as [14, 15]:

$$\sigma_g^2[s'_n(x, y)] = \frac{N_x N_y \langle V^2 \rangle}{n w_x^2 w_y^2 \Delta t} K \quad (1.20)$$

where  $s'_n$  is the inverse Fourier transformed signal with  $n$  averages and  $K$  is a factor depending on the filter characteristics.

### 1.3 Noise distribution in MRI

As discussed earlier, the acquired raw complex MR data in the presence of thermal noise in the  $k$  - space is characterized by a Gaussian probability density function (PDF). The  $k$  - space data is then Fourier transformed to obtain the magnetization distribution. The data distribution in the real and imaginary components will still be Gaussian due to the linearity and the orthogonality of the Fourier transform. However, complex images as such is not used for any analysis. To use both parts of the complex data values, we calculate magnitude images and phase images. This thesis mainly deals with the magnitude images, so phase images will not be discussed further. Since the computation of magnitude image is a non linear operation the noise distribution in the magnitude image will be no longer Gaussian but Rician distributed.

The magnitude image  $M$ , is computed as the root Sum of Squares (SoS) of the real and imaginary part of the complex signal for each pixel, which can be written as:

$$M(\mathbf{x}) = \sqrt{R(\mathbf{x})^2 + I(\mathbf{x})^2} \quad (1.21)$$

The derivation of the PDF of the resulting distribution of  $M$  is discussed in the remaining part of this section. Let  $m_r$  and  $m_i$  be the means and  $\sigma_g^2$  the variance of the Gaussian random variables  $R$  and  $I$  respectively. Then the PDF of the random variables  $Y_1 = R^2$  and  $Y_2 = I^2$  can be written as [16]:

$$P_{Y_1}(y_1) = \frac{1}{\sqrt{2\pi y_1} \sigma_g} e^{-\frac{y_1 + m_r^2}{2\sigma_g^2}} \cosh\left(\frac{\sqrt{y_1} m_r}{\sigma_g^2}\right), y_1 \geq 0 \quad (1.22)$$

and

$$P_{Y_2}(y_2) = \frac{1}{\sqrt{2\pi}y_2\sigma_g} e^{-\frac{y_2+m_r^2}{2\sigma_g^2}} \cosh\left(\frac{\sqrt{y_2}m_i}{\sigma_g}\right), y_2 \geq 0 \quad (1.23)$$

respectively. The characteristic functions corresponding to Eqns.(1.22) and (1.23) are:

$$\psi_{Y_1}(jv) = \frac{1}{(1 - j2v\sigma_g^2)^{1/2}} e^{\frac{jm_r^2v}{1-2v\sigma_g^2}} \quad (1.24)$$

and

$$\psi_{Y_2}(jv) = \frac{1}{(1 - j2v\sigma_g^2)^{1/2}} e^{\frac{jm_i^2v}{1-2v\sigma_g^2}} \quad (1.25)$$

respectively. Now let  $Y = R^2 + I^2$ . The corresponding characteristic function can be written as:

$$\psi_Y(jv) = \frac{1}{(1 - j2v\sigma_g^2)} e^{\frac{jv(m_r^2+m_i^2)}{1-2v\sigma_g^2}} \quad (1.26)$$

This characteristic function can be inverse Fourier transformed to yield the PDF of  $Y$ :

$$p_Y(y) = \frac{1}{2\sigma_g^2} e^{-\frac{a^2+y}{2\sigma_g^2}} I_0\left(\sqrt{y}\frac{a}{\sigma_g}\right), y \geq 0 \quad (1.27)$$

where  $a^2 = m_r^2 + m_i^2$  and  $I_0$  is the 0<sup>th</sup> order modified bessel function of the first kind. Now, we define a new random variable  $M = \sqrt{Y}$ . The PDF of  $M$ , obtained from Eq.(1.27) by a simple change of variable, is [16]

$$p_M(m) = \frac{m}{\sigma_g^2} e^{-\frac{m^2+a^2}{2\sigma_g^2}} I_0\left(\frac{ma}{\sigma_g}\right), m \geq 0 \quad (1.28)$$

This is the PDF of the Rician-distributed random variable  $M$ . The shape of the Rician distribution depends on the signal to noise ratio(SNR), which is here defined as the ratio  $a/\sigma_g$ . Fig. 1.2 shows the Rice PDF as a function of the magnitude  $m$  for various values of the SNR. In Fig. 1.3, the histogram of the background region of the real, imaginary and magnitude images shown in Fig. 1.1 is displayed. The Gaussian and Rician nature of the data distribution in complex and magnitude images can also be observed from these true images. In Fig. 1.4, the distributions of pixels in different regions of a simulated noisy MR image is displayed.

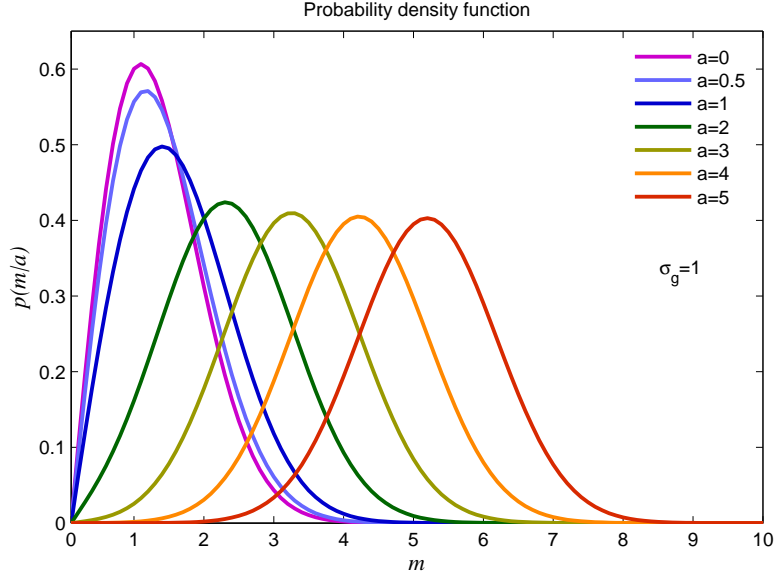


Figure 1.2: Rician PDF for different SNR values.

The  $k^{\text{th}}$  raw moment of the Rice PDF can be analytically expressed as a function of the confluent hypergeometric function of the first kind, denoted by  ${}_1F_1$ :

$$E[M^k] = (2\sigma_g^2)^{k/2} \Gamma \left( 1 + \frac{k}{2} \right) {}_1F_1 \left[ -\frac{k}{2}; 1; -\frac{a^2}{2\sigma_g^2} \right] \quad (1.29)$$

where  $\Gamma$  represents the Gamma function. The first few moments of the Rice PDF are given below

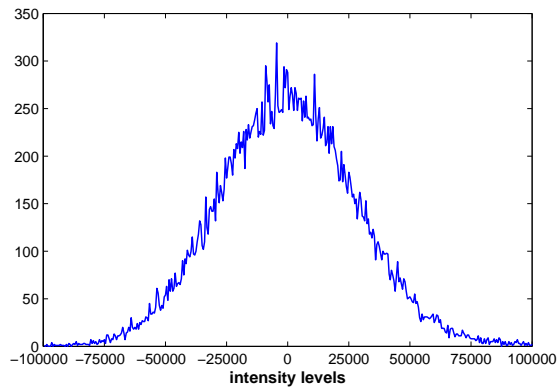
$$E[M] = \sigma_g \sqrt{\frac{\pi}{2}} e^{-\frac{a^2}{4\sigma_g^2}} \left[ \left( 1 + \frac{a^2}{2\sigma_g^2} \right) I_0 \left( \frac{a^2}{4\sigma_g^2} \right) + \frac{a^2}{2\sigma_g^2} I_1 \left( \frac{a^2}{4\sigma_g^2} \right) \right] \quad (1.30)$$

$$E[M^2] = a^2 + 2\sigma_g^2 \quad (1.31)$$

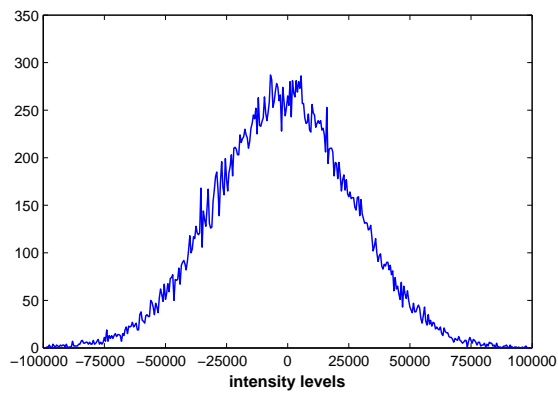
$$E[M^3] = \sigma_g^3 \sqrt{\frac{\pi}{2}} e^{-\frac{a^2}{4\sigma_g^2}} \left[ \left( 3 + 3\frac{a^2}{\sigma_g^2} + \frac{a^4}{2\sigma_g^4} \right) I_0 \left( \frac{a^2}{4\sigma_g^2} \right) + \left( 2\frac{a^2}{\sigma_g^2} + \frac{a^4}{2\sigma_g^4} \right) I_1 \left( \frac{a^2}{4\sigma_g^2} \right) \right] \quad (1.32)$$

$$E[M^4] = a^2 + 8\sigma_g^2 a^2 + 8\sigma_g^4 \quad (1.33)$$

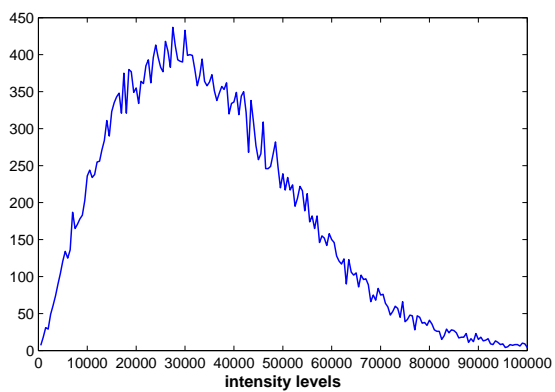
### 1.3. Noise distribution in MRI



(a)



(b)



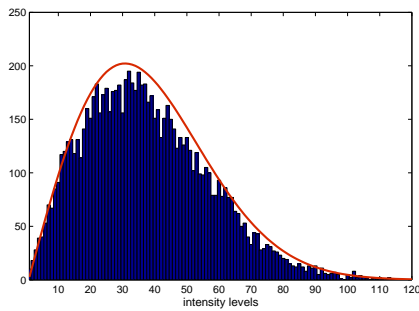
(c)

Figure 1.3: Histogram of the background region of the Kiwi fruit in Fig.1.1 (a) histogram of the real part (b) histogram of the imaginary part (c) histogram of the magnitude image.

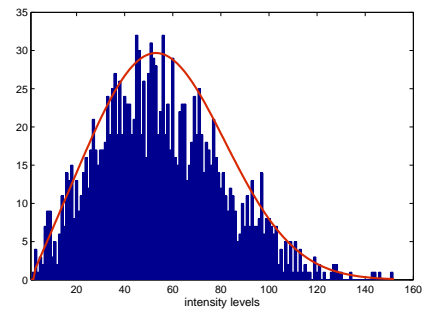
### 1.3. Noise distribution in MRI



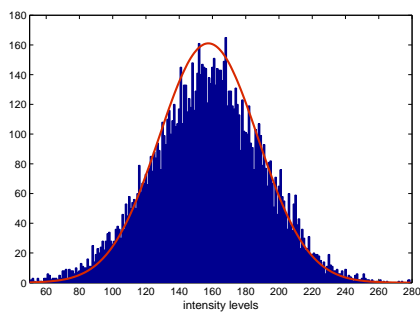
(a)



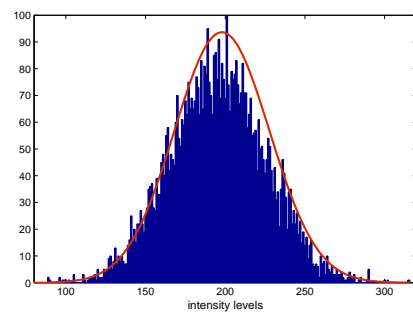
(b)



(c)



(d)



(e)

Figure 1.4: Distribution of pixels in different regions of a simulated noisy MR image (a) simulated noisy MR images with noise level  $\sigma_g = 30$ , (b) distribution of pixels in the background region (c) distribution of pixels in the CSF region (d) distribution of pixels in the grey matter region (e) distribution of pixels in the white matter region.

When  $a = 0$ , the Rice distribution becomes a Rayleigh distribution and the corresponding PDF can be written as:

$$p_M(m) = \frac{m}{\sigma_g^2} e^{-\frac{m^2}{2\sigma_g^2}}, m \geq 0 \quad (1.34)$$

The raw moments of the Rayleigh PDF can be analytically expressed as:

$$E[M^k] = (2\sigma^2)^{k/2} \Gamma\left(1 + \frac{k}{2}\right) \quad (1.35)$$

The first four moments of the Rayleigh PDF are explicitly given by:

$$E[M] = \sigma_g \sqrt{\frac{\pi}{2}} \quad (1.36)$$

$$E[M^2] = 2\sigma_g^2 \quad (1.37)$$

$$E[M^3] = 3\sigma_g^3 \sqrt{\frac{\pi}{2}} \quad (1.38)$$

$$E[M^4] = 8\sigma_g^4 \quad (1.39)$$

In the MR image background, where the SNR is zero due to the lack of water-proton density in the air, the data will follow a Rayleigh distribution.

At high SNR, i.e. when  $a/\sigma_g \rightarrow \infty$ , the Rician distribution approaches a Gaussian distribution. The asymptotic expansion of the Bessel function  $I_0(x)$  when  $x$  is large is

$$I_0(x) \sim \frac{e^x}{\sqrt{2\pi x}} \quad (1.40)$$

then the Rice PDF in Eq. (1.28) can be written as:

$$p_M(m) = \frac{1}{\sigma_g \sqrt{2\pi}} e^{-\frac{(m-a)^2}{2\sigma_g^2}} \quad (1.41)$$

which is the PDF for Gaussian distribution.

Acquisition of MR images with multiple-coils are becoming common nowadays. When MR images are acquired with multiple coils and reconstructed using SoS, the composite magnitude signal  $M_L(\mathbf{x})$  can be written as [17, 18]

$$M_L(\mathbf{x}) = \sqrt{\sum_{l=1}^L R_l(\mathbf{x})^2 + I_l(\mathbf{x})^2} \quad (1.42)$$

where  $L$  is the number of coils. The PDF of the composite magnitude image  $M_L$  can be derived in a similar manner as in the case for Rice distribution. Assuming  $Y = \sum_{l=1}^L R_l^2 + I_l^2$ , the characteristic function of  $Y$  can be written as:

$$\psi_Y(j\nu) = \frac{1}{(1 - j2\nu\sigma_g^2)^L} e^{\frac{j\nu(\sum_{l=1}^L m(l)_r^2 + m(l)_i^2)}{1 - 2\nu\sigma_g^2}} \quad (1.43)$$

The corresponding PDF after the inverse Fourier transform is:

$$p_Y(y) = \frac{1}{2\sigma_g^2} \left(\frac{y}{a^2}\right)^{(L-1)/2} e^{-\frac{a^2+y}{2\sigma_g^2}} I_{L-1}\left(\sqrt{y}\frac{a}{\sigma_g}\right), y \geq 0 \quad (1.44)$$

where  $a^2 = \sum_{l=1}^L m(l)_r^2 + m(l)_i^2$  and  $I_{L-1}$  is the  $L - 1^{th}$  order modified bessel function of the first kind. Now, if we define a new random variable  $M_L = \sqrt{Y}$ , the PDF of  $M_L$  can be written as

$$p_{M_L}(m) = \frac{m^L}{\sigma_g^2 a^{L-1}} e^{-\frac{m^2+a^2}{2\sigma_g^2}} I_{L-1}\left(\frac{ma}{\sigma_g}\right), m \geq 0 \quad (1.45)$$

The PDF given in Eq. (1.36) is the PDF of the generalized Rice distribution or also known as the PDF of the non central chi (nc- $\chi$ ) distribution. The  $k^{th}$  moment of  $M_L$  is given by [16]:

$$E[M_L^k] = (2\sigma_g^2)^{k/2} e^{-a^2/2\sigma_g^2} \frac{\Gamma(\frac{2L+k}{2})}{\Gamma(L)} {}_1F_1\left[\frac{2L+k}{2}; L; \frac{a^2}{2\sigma_g^2}\right] \quad (1.46)$$

The first two even moments of the nc- $\chi$  PDF can be written as :

$$E[M_L^2] = a^2 + 2L\sigma_g^2 \quad (1.47)$$

and

$$E[M_L^4] = a^4 + 4(L+1)a^2\sigma_g^2 + 4L(L+1)\sigma_g^4 \quad (1.48)$$

In the background, the non central chi (nc- $\chi$ ) distribution simplifies to a central chi distribution and as SNR increases, nc- $\chi$  distribution approaches a Gaussian distribution. The PDF of the central chi distribution (or the generalized Rayleigh distribution) is given by:

$$p_{M_L}(m) = \frac{m^{2L-1}}{2^{L-1}\sigma_g^{2L}\Gamma(L)} e^{-\frac{m^2}{2\sigma_g^2}}, m \geq 0 \quad (1.49)$$

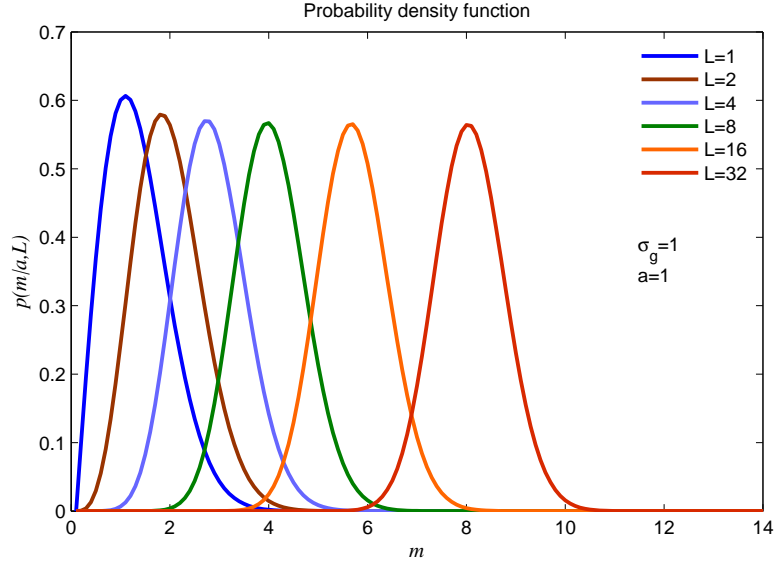


Figure 1.5: nc- $\chi$  PDF for different values of L.

The  $k^{th}$  moment of the central chi PDF is given by:

$$E[M_L^k] = (2\sigma_g^2)^{\frac{k}{2}} \frac{\Gamma(\frac{2L+k}{2})}{\Gamma(L)} \quad (1.50)$$

The main moments of the central chi PDF are given below.

$$E[M_L] = \sqrt{2} \frac{\Gamma(L + 1/2)}{\Gamma(L)} \sigma_g^3 \quad (1.51)$$

$$E[M_L^2] = 2L\sigma_g \quad (1.52)$$

$$E[M_L^3] = 3\sqrt{2} \frac{\Gamma(L + 3/2)}{\Gamma(L)} \sigma_g \quad (1.53)$$

$$E[M_L^4] = 4L(L + 1)\sigma_g^4 \quad (1.54)$$

Fig. 1.5 shows the PDF of the nc- $\chi$  distribution with different values of L.

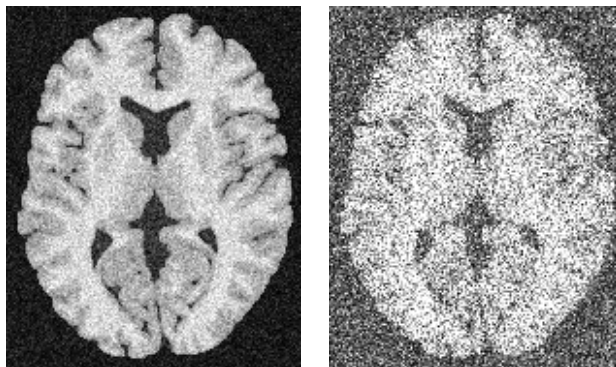
## 1.4 Main contributions

The main contributions presented in this thesis are:

- Methods to estimate the noise level from the MR images in the absence of background region are proposed. Most of the methods proposed earlier exploited the Rayleigh distributed background region in the MR images to estimate the noise. The performance of these methods depends on the level of noise and the availability of the background region. For e.g. the methods in [19, 20, 21, 22] estimates the noise variance from the background mode of the image histogram. These methods are based on the observation that the regions representing the background and signal can be easily distinguishable from the image histogram. However when the noise is too high, estimation with these methods will be a problem since it becomes difficult to distinguish the background and signal region from the histogram. This is demonstrated in Fig. 1.6. Also the presence of artifacts (e.g. Ghost artifacts) can influence the estimation for the methods based on background region. For e.g., the images given in Fig. 1.7 is a challenging one for background based methods. However, the most important factor is that none of the background region based methods will work in the absence or with very less background region. The proposed methods in this thesis are object based methods that doesn't depend on the background region for noise estimation.
- A maximum likelihood (ML) estimation method to denoise MR images corrupted with Rician noise is proposed. In the early days, many authors applied the conventional classical denoising techniques to denoise MRI. These methods assumed the noise in the MRI as Gaussian. The major drawback of these methods are that the biasing effects of Rician noise was not taken into account. This bias will increase with decreasing SNR. This is demonstrated in Fig. 1.8. Later many methods were proposed to denoise MR images. Most of these methods exploited the second moment of the Rice distribution to reduce the bias in the denoised images. i.e. the image is denoised with the methods based on the Gaussian assumption and to reduce the bias,  $2\sigma_g^2$  is subtracted from the squared denoised image. However, in [23] it is shown that the sample size and SNR has a significant influence on the process of estimating the true underlying

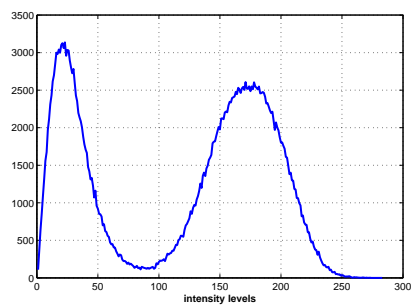
signal using this approach. ML methods were proved to be better than the aforementioned methods. Conventionally for MR image denoising, ML estimation methods incorporate the Rice distribution to estimate the true, underlying signal from a local neighborhood within which the signal is assumed to be constant. However, if this assumption is not met, such filtering will lead to blurred edges and loss of fine structures in the image. In this thesis, as a solution to this problem, we put forward the concept of restricted local neighborhoods, where the true intensity for each noisy pixel is estimated using ML estimation method from a set of preselected neighboring pixels.

- A method to denoise MR images acquired with multiple coils is put forward. Many methods have been proposed in the literature for MRI noise estimation and denoising. However, not many approaches were suggested for estimating the noise or underlying true signal from MR images acquired with multichannel surface-coil arrays. For multiple coil systems, the data distribution depends on the reconstruction techniques used. However, if the magnitude image from surface-coil arrays are reconstructed as the root sum of squares, in the absence of noise correlations and subsampling, the data is assumed to follow a non central- $\chi$  (nc- $\chi$ ) distribution. Even though, multiple coil systems were initially developed to enhance the SNR of the acquired images (the smaller the sensitive volume of a coil, the lower the noise from the adjacent structures and better the SNR will be), later parallel MRI (pMRI) techniques were employed to it to accelerate the acquisition process through  $k$ -space subsampling (in the phase encoding direction). The subsampling of  $k$ -space and the correlations between the data from different coils makes the noise level in the image spatially varying. In this thesis, we propose a method based on the non local ML estimation for the estimation of the noise level and underlying true signal from multiple-coil acquired MR images. Both the nc- $\chi$  distribution and the spatially varying nature of the noise is taken into account in the proposed method.

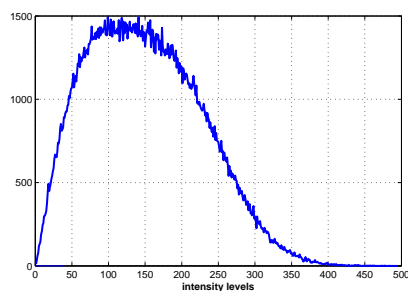


(a)

(b)

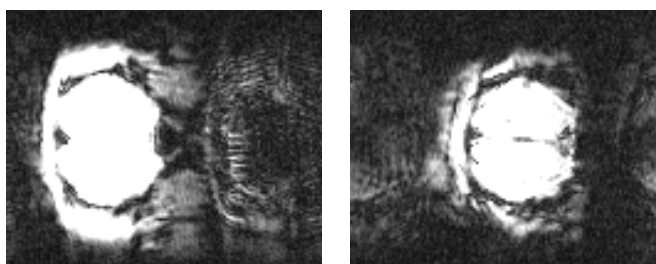


(c)



(d)

Figure 1.6: Issues with histogram based methods for noise estimation (a) and (b) noisy images with a noise level of  $\sigma_g = 20$  and  $\sigma_g = 60$  respectively (c) and (d) corresponding histograms.



(a)

(b)

Figure 1.7: Images with artifacts in the background region

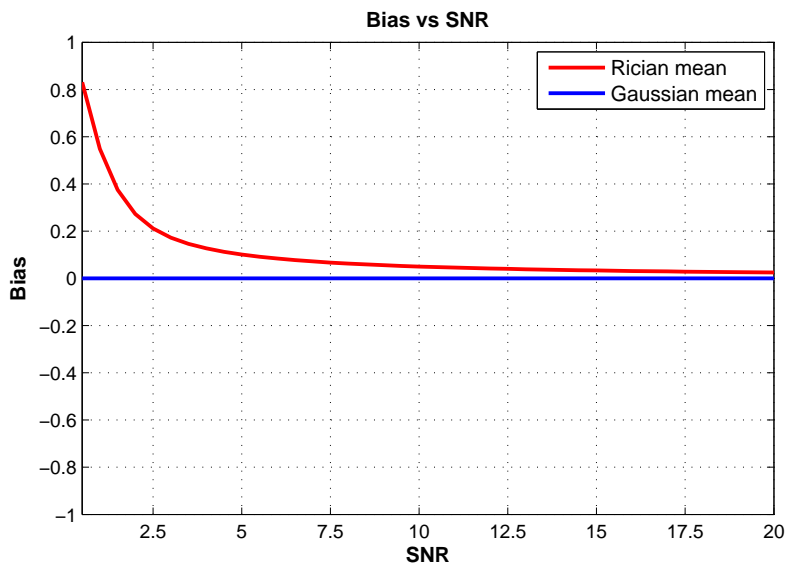


Figure 1.8: Rician Bias : This experiment was conducted with  $\sigma_g = 1$  and varying  $a$  from 0.5 to 20

## 1.5 Thesis organization

The thesis is structured as follows:

- **Chapter 1** is the present chapter, which introduces the purpose of this thesis and gives an overview of MRI.
- **Chapter 2** presents object based methods to estimate noise from MR images. Two new methods based on the local ML estimation and local skewness based estimation of the noise variance are introduced in this chapter.
- **Chapter 3** presents a restricted local ML estimation method to denoise MR images corrupted with Rician noise. Conventionally, ML methods incorporate the Rice distribution to estimate the true, underlying signal from a local neighborhood within which the signal is assumed to be constant. However, if this assumption is not met, such filtering will lead to blurred edges and loss of fine structures. As a solution to this problem, we put forward the concept of restricted local neighborhoods where the

true intensity for each noisy pixel is estimated from a set of preselected neighboring pixels.

- **Chapter 4** presents a method to estimate the noise and underlying true signal from MR images acquired with multiple coils. Even though many methods were proposed to denoise MR images, only few deal with the estimation of true signal from MR images acquired with multiple coils. The proposed method take care of  $nc$ - $\chi$  distributed noise, which arises when using SoS reconstruction, and also the spatially varying nature of the noise which is common in SENSE and GRAPPA reconstructed images.

### References

- [1] I. I. Rabi, J. R. Zacharias, S. Millman, and P. Kusch, “A new method of measuring nuclear magnetic moment,” *Phys. Rev*, vol. 53, pp. 318, 1938.
- [2] F. Bloch, W. W. Hansen, and M. Packard, “The nuclear induction experiment,” *Physical Review*, vol. 70, pp. 474–485, 1946.
- [3] F. Bloch, “Nuclear induction,” *Physical Review*, vol. 70, pp. 460–474, 1946.
- [4] E. M. Purcell, H. C. Torrey, and R. V. Pound, “Resonance absorption by nuclear magnetic moments in a solid,” *Physical Review*, vol. 69, pp. 37, 1946.
- [5] R. V. Damadian, “Tumor detection by nuclear magnetic resonance,” *Science*, vol. 171, pp. 1151, 1971.
- [6] P. C. Lauterbur, “Image formation by induced local interactions: examples employing nuclear magnetic resonance,” *Nature*, vol. 242, pp. 190, 1973.
- [7] A. Kumar, D. Welte, and R. R. Ernst, “NMR fourier zeugmatography,” *J Magn Reson*, vol. 18, no. 1, pp. 69–83, 1975.

- [8] P. Mansfield, “Multi-planar image formation using nmr spin echoes,” *J. Phys. C : Solid State Physics*, vol. 10, pp. L55–L58, 1977.
- [9] V. Kuperman, *Magnetic Resonance Imaging - Physical Principles and Applications*, Academic Press, 2000.
- [10] M. A. Brown and R. C. Semelka, *MRI - Basic Principles and Applications*, John Wiley and Sons, Inc., 2003.
- [11] D. G. Nishimura, *Principles of Magnetic Resonance Imaging*, Standard University, 2010.
- [12] J. Sijbers, A. J. den Dekker, M. Verhoye, J. Van Audekerke, and D. Van Dyck, “Estimation of noise from magnitude MR images,” *Magn Reson Imaging*, vol. 16, no. 1, pp. 87–90, 1998.
- [13] A. Macovski, “Noise in MRI,” *Magn Reson Med*, vol. 36, pp. 494–497, 1996.
- [14] D. L. Parker and G. T. Gullberg, “Signal-to-noise efficiency in magnetic resonance imaging,” *Med Phys*, vol. 17, no. 2, pp. 250–257, 1990.
- [15] J. Sijbers, *Estimation of Signal and Noise from Magnitude MR Images*, Ph.D. thesis, University of Antwerp, May 1998, Info: <http://webhost.ua.ac.be/visielab/sijbers/thesis.html>.
- [16] John. G. Proakis, *Digital Communications*, Mc Graw Hill, 2001.
- [17] C. D. Constantinides, E. Atalar, and E. R. McVeigh, “Signal-to-noise measurements in magnitude images from NMR phased arrays,” *Magn Reson Med*, vol. 38, pp. 852–857, 1997.
- [18] S. Aja-Fernández, A. Tristán, and C. Alberola-López, “Noise estimation in single and multiple coil magnetic resonance data based on statistical models,” *Magn Reson Imaging*, vol. 27, pp. 1397–1409, 2009.
- [19] G.M.P. van Kempen and L.J. van Vliet, “The influence of the background estimation on the superresolution properties of non-linear image restoration algorithms,” in *Three-Dimensional and Multidimensional*

- Microscopy: Image Acquisition and Processing VI: Proceedings of SPIE Progress in Biomedical Optics*, D. Cabib, C.J. Cogswell, J.A. Conchello, J.M. Lerner, and T. Wilson, Eds., 1999, vol. 3605, pp. 179–189.
- [20] M. E. Brummer, R. M. Mersereau, R.L. Eisner, and R.R.J. Lewine, “Automatic detection of brain contours in MRI data sets,” *IEEE Trans Med Imaging*, vol. 12, no. 2, pp. 153–168, 1993.
- [21] Lin-Ching Chang, Gustavo K. Rohde, and Carlo Pierpaoli, “An automatic method for estimating noise-induced signal variance in magnitude-reconstructed magnetic resonance images,” in *SPIE Medical Imaging 2005: Image Processing*, April 2005, vol. 5747, pp. 1136–1142.
- [22] J. Sijbers, D. Poot, A. J. den Dekker, and W. Pintjens, “Automatic estimation of the noise variance from the histogram of a magnetic resonance image,” *Phys Med Biol*, vol. 52, pp. 1335–1348, 2007.
- [23] J. Sijbers, A. J. den Dekker, P. Scheunders, and D. Van Dyck, “Maximum likelihood estimation of Rician distribution parameters,” *IEEE Trans. Med. Imag.*, vol. 17, no. 3, pp. 357–361, June 1998.

# Noise estimation from MR images

---

## Contents

---

<b>2.1</b>	<b>Introduction</b>	24
<b>2.2</b>	<b>Methods</b>	26
2.2.1	Noise estimation using local maximum likelihood estimation	28
2.2.2	Noise estimation using measurement of local skewness	29
<b>2.3</b>	<b>Experimental Results</b>	33
<b>2.4</b>	<b>Conclusion</b>	37

---

The work described in this chapter has been published as:

**J. Rajan**, D. Poot, J. Juntu, and J. Sijbers, “Noise measurement from magnitude MRI using local estimates of variance and skewness”, *Physics in Medicine and Biology*, vol 55, pp N441- N449, 2010

### Abstract:

In this chapter, we address the estimation of the noise level in magnitude MR images in the absence of background data. Most of the methods proposed earlier exploited the Rayleigh distributed background region in the MR images to estimate the noise level. These methods, however, cannot be used for images where no background information is available. We propose two different approaches for noise estimation in the absence of image background.

The first method is based on the local estimation of the noise variance using ML estimation and the second method is based on the local estimation of the skewness of the magnitude data distribution. Experimental results on synthetic and real MR image data sets show that the proposed estimators accurately estimate the noise level in a magnitude MR image.

## 2.1 Introduction

Estimation of the noise variance from MR images is often of key importance as the noise variance is an input parameter for many image post-processing tasks such as noise reduction, segmentation, parameter estimation, or clustering [1, 2, 3, 4]. The estimated noise variance also gives a measure of the quality of the MR data and could potentially help in improving the design of scanners [5]. Noise in the MRI can be estimated from either complex or magnitude images. However, it is a common practice to work with magnitude and phase images instead as they have more physical meaning (proton density, flow, etc) [6]. Also, complex images are not always available as the usual output of the scanners are magnitude images. As discussed in the previous chapter, magnitude MR data in the presence of noise can be well modeled by a Rician distribution when the images are acquired using single coil, but may not follow Rician distribution when multiple-coils are used for data acquisition. In this chapter, we consider only the cases where the Rician model can be used.

The straight forward and most reliable approach to estimate noise from the magnitude images is to use a double acquisition method. When two images of the same subject are acquired under identical imaging conditions, noise variance can be estimated using the averaged and single images [6]. However, it is not always possible to acquire the same measurement twice. For. e.g., time-sensitive acquisitions in contrast material-enhanced studies, functional studies or studies with limited imaging time, experiments cannot be repeated to derive the image noise [7]. In those cases, noise has to be estimated from single images.

In the past, many methods have been proposed in the literature for the estimation of the noise level from single magnitude MR images [8, 1, 9, 10, 4].

A survey of these methods are given in Aja-Fernández et al. [11]. Most of the methods proposed earlier estimate the noise level from the background area of the magnitude MR images where the noise follows Rayleigh distribution due to the absence of signal [12]. Unfortunately, these methods cannot be used for images where no background information is available. For MR images other than the brain, like cardiac or lung images, background data may not be available. For example, in case the field of view (FoV) is small, such that noise assumptions based on Rayleigh distribution fail [11]. Also, the new scanning techniques and software eliminates most part of the noisy background, which in fact affect the methods based on Rayleigh model that need a certain amount of background pixels to perform proper estimation [13]. The above mentioned issues with the methods based on the Rayleigh model drives the need to develop methods that doesn't depend on the background region for noise estimation. Recently, Aja-Fernández et al. in [4] proposed a method that doesn't rely on the background region to estimate the noise level in MR images. Their method was based on the assumption that there exists many high SNR regions in the image. Since Rician distribution approaches a Gaussian distribution at high SNR, the noise variance can be estimated from these regions. However, at low SNR, the Rician distribution is not approximated well by a Gaussian distribution, causing a bias in the estimated noise level.

In this chapter, we propose two different approaches to address the aforementioned issues related to the Rician noise estimation. The first method is based on the ML estimation of the local variance for each pixel of the image using a local neighborhood. The global noise variance can then be computed from the mode of the distribution of the estimated local variance. The ML method simultaneously estimates the underlying true signal and noise variance from the Rician distributed data if the underlying signal is constant [14]. It will be experimentally shown that the proposed method based on local ML estimation of variance is highly accurate in estimating the noise level, but has a rather high computational complexity. Therefore, a computationally more efficient method is also proposed. This method is based on the local skewness. A correction factor for the variance estimated with the Gaussian assumption

is introduced based on the estimated skewness for the actual computation of the noise standard deviation  $\sigma_g$ .

## 2.2 Methods

When enough background region is present in the image, noise level can be directly estimated from the pixels in these regions. Let  $M_B$  represents the non-signal background area in the MR image. Then based on the first moment of the Rayleigh distribution (ref :Eq.1.36), the noise level can be estimated as:

$$\hat{\sigma}_g = \sqrt{\frac{2}{\pi}} \langle M_B \rangle \quad (2.1)$$

where  $\hat{\sigma}_g$  is the estimated noise standard deviation and  $\langle M_B \rangle$  represents the mean of the Rayleigh background region. Even though it is a straightforward and simple approach, the drawback of this approach is the requirement of an explicit segmentation algorithm for extracting the background. In addition, conventional segmentation methods might not work properly when the noise level is too high and/or in diffusion weighted MR images, where the scalp regions are sometimes misclassified as background regions[15]. Background segmentation with a conventional segmentation algorithm is shown in Fig. 2.1. Even though its performance is acceptable for the given simulated image, remains of the object is evident in the segmented background region of the diffusion weighted image. Also, artifacts(e.g.Ghost artifacts) can influence the estimation. Many methods were proposed to estimate the noise variance from the image background without explicit segmentation. [8, 16, 17, 10, 4] are to name a few. In [8], [16], [17] and [10] the noise variance were estimated from the background mode of the image histogram. These methods are based on the observation that the regions representing the background and signal can be easily distinguishable from the image histogram. These methods work well at reasonable noise levels. However when the noise is too high, estimation with these methods will be a problem since it becomes difficult to distinguish the background and the signal region from the histogram. A more robust

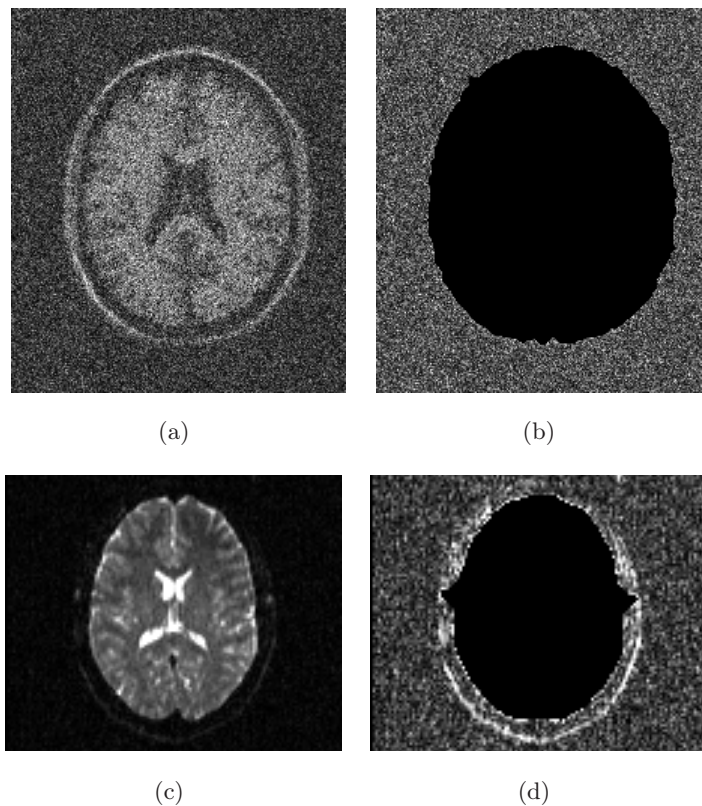


Figure 2.1: Background segmentation from MR images (a) and (c) noisy MR images with Rayleigh background (b) and (d) segmented background regions.

method was the one based on local statistics proposed in [4]:

$$\hat{\sigma}_g = \sqrt{\frac{2}{\pi}} \text{mode}\{\langle M(i) \rangle\} \quad (2.2)$$

where  $\langle M(i) \rangle$  corresponds to the local mean computed for each pixel at location  $i$ .

However, none of the aforementioned methods work in the absence of background region. In [4], a method is proposed to estimate the noise level in the absence of background region. This is based on the fact that at high SNR the Rician distribution approaches normal distribution. In that case, the noise standard deviation can be estimated from high SNR homogeneous regions. If there exists many such piecewise homogeneous high SNR regions, the noise can be estimated automatically without manually selecting a region

of interest as [4]:

$$\widehat{\sigma}_g^2 = \text{mode}\{\sigma_{M(i)}^2\}, \quad (2.3)$$

where  $\widehat{\sigma}_g^2$  is the variance of the estimated noise and  $\sigma_{M(i)}^2$  corresponds to the local variance computed around each pixel at  $i$ . However, at low SNR, Eq. (2.3) will lead to an under estimation of the noise level. In section 2.2.1, we discuss how to measure the noise variance from an MR image without depending on high SNR or background regions.

### 2.2.1 Noise estimation using local maximum likelihood estimation

Let  $m_1, m_2, \dots, m_n$  be  $n$  statistically independent observations from a region of constant signal intensity  $a$ . Then the joint pdf of the observations can be written as [9]

$$p(\{m_i\}|a) = \prod_{i=1}^n \frac{m_i}{\sigma_g^2} e^{-\frac{m_i^2 + a^2}{2\sigma_g^2}} I_0\left(\frac{am_i}{\sigma_g^2}\right) \quad (2.4)$$

Given the observed data and a model of interest the unknown parameters in the pdf can be estimated by maximizing the corresponding likelihood function. Therefore the ML estimate of the underlying signal amplitude  $a$  and noise variance  $\sigma_g^2$  can now be computed by maximizing the likelihood function  $\mathcal{L}(a)$  or equivalently  $\ln \mathcal{L}(a)$ , with respect to  $a$  and  $\sigma_g^2$ :

$$\ln \mathcal{L} = \sum_{i=1}^n \ln \left( \frac{m_i}{\sigma_g^2} \right) - \sum_{i=1}^n \frac{m_i^2 + a^2}{2\sigma_g^2} + \sum_{i=1}^n \ln I_0 \left( \frac{am_i}{\sigma_g^2} \right) \quad (2.5)$$

The ML estimate is then found from the global maximum of  $\ln \mathcal{L}$  w.r.t.  $a$  and  $\sigma_g^2$  [9]:

$$\{\widehat{a}_{\text{ML}}, \widehat{\sigma}_{\text{ML}}^2\} = \arg\{\max_{a, \sigma_g^2}(\ln \mathcal{L})\} \quad (2.6)$$

The above procedure assumes the underlying signal to be constant within the local neighborhood from which the signal and noise variance is estimated. If this assumption is valid for most of the local pixel neighborhoods, a robust estimator of the noise variance is given by the mode of all ML estimated local noise levels:

$$\widehat{\sigma}_m^2 = \text{mode}\{\widehat{\sigma}_{ML(i)}^2\}, \quad (2.7)$$

where  $\widehat{\sigma}_m^2$  is the estimated noise variance and  $\widehat{\sigma}_{ML(i)}^2$  is the local ML estimate of the noise variance at each pixel  $i$ . In fact, most of the MR images are piecewise constant with a reasonably small number of classes (e.g. MR image of brain) [18]. Since the noise is estimated from the available piecewise constant regions in the image, this method neither depends on the image background nor on the high SNR regions of the image.

### 2.2.2 Noise estimation using measurement of local skewness

Even though the method based on local ML estimation is accurate, a drawback is its time complexity. In this section, we propose a method based on the local computation of the skewness of the magnitude data distribution to estimate the noise variance. The variance of the Rician distribution in terms of the moments can be written as

$$\sigma_r^2 = E[M^2] - E[M]^2 \quad (2.8)$$

where

$$E[M] = \sigma_g \sqrt{\frac{\pi}{2}} e^{-\frac{a^2}{4\sigma_g^2}} \left[ \left(1 + \frac{a^2}{2\sigma_g^2}\right) I_0\left(\frac{a^2}{4\sigma_g^2}\right) + \frac{a^2}{2\sigma_g^2} I_1\left(\frac{a^2}{4\sigma_g^2}\right) \right] \quad (2.9)$$

and

$$E[M^2] = a^2 + 2\sigma_g^2 \quad (2.10)$$

Expanding Eq. (2.8) we will get:

$$\sigma_r^2 = a^2 + 2\sigma_g^2 - \left( \sigma_g \sqrt{\frac{\pi}{2}} e^{-\frac{a^2}{4\sigma_g^2}} \left[ \left(1 + \frac{a^2}{2\sigma_g^2}\right) I_0\left(\frac{a^2}{4\sigma_g^2}\right) + \frac{a^2}{2\sigma_g^2} I_1\left(\frac{a^2}{4\sigma_g^2}\right) \right] \right)^2 \quad (2.11)$$

It is difficult to derive an expression for  $\sigma_g^2$  from Eq. (2.11) due to the presence of Bessel functions. However, when the noise follows a Rayleigh or Gaussian distribution (at low or high SNR), Eq. (2.11) will reduce to simple equations:

$$\sigma_g^2 = \sigma_r^2 \left(2 - \frac{\pi}{2}\right)^{-1} \quad (2.12)$$

and

$$\sigma_g^2 = \sigma_r^2 \quad (2.13)$$

respectively. In general,  $\sigma_g^2$  can be computed by multiplying  $\sigma_r^2$  with a correction factor [19]. In this work, we propose a correction factor based on skewness of the Rician distribution :

$$\sigma_g^2 = \sigma_r^2 \times \varphi(\mathcal{S}) \quad (2.14)$$

where  $\varphi(\mathcal{S})$  is the correction factor which is a function of the skewness  $\mathcal{S}$  of the Rician distribution and is in the range  $[1, (2 - \pi/2)^{-1}]$ . i.e. when the Rician distribution approaches a Rayleigh distribution (at low SNR), the correction factor tends to  $(2 - \pi/2)^{-1}$  and when the Rician distribution approaches a Gaussian (at high SNR), the correction factor tends to 1. The proximity of the Rician distribution towards Rayleigh or Gaussian can be measured using its skewness, which is defined by:

$$\mathcal{S} = \frac{2E[M]^3 - 3E[M]E[M^2] + E[M^3]}{(E[M^2] - E[M]^2)^{\frac{3}{2}}} \quad (2.15)$$

where

$$E[M^3] = \sigma_g^3 \sqrt{\frac{\pi}{2}} e^{-\frac{a^2}{4\sigma_g^2}} \left[ \left( 3 + 3\frac{a^2}{\sigma_g^2} + \frac{a^4}{2\sigma_g^4} \right) I_0 \left( \frac{a^2}{4\sigma_g^2} \right) + \left( 2\frac{a^2}{\sigma_g^2} + \frac{a^4}{2\sigma_g^4} \right) I_1 \left( \frac{a^2}{4\sigma_g^2} \right) \right] \quad (2.16)$$

$\mathcal{S}$  can now be analytically computed using Eq. (2.15). The skewness of the Rician distribution is a monotonically decreasing function of the SNR, defined as  $a/\sigma_g$ , with values range from 0.631 (for SNR=0) to 0 (for SNR= $\infty$ ). Hence, the correction factor  $\varphi$  at various SNR can be computed by exploiting the skewness of the Rician distribution. The skewness and correction factor as a function of SNR is depicted in Fig. 2.2 and Fig. 2.3 respectively.

Now, if we keep  $\sigma_g$  constant and vary the value of  $a$  from zero to a high value we can compute  $\varphi$  ( $\varphi = \sigma_g^2/\sigma_r^2$ ) for every value of  $\mathcal{S}$  from 0.631 to 0. The value of  $\sigma_r^2$  is calculated using Eq. (2.8). This relationship is shown in Fig. 2.4. A lookup table can then be created to represent this relationship. Now, for every  $\mathcal{S}$ , a corresponding value for  $\varphi$  can be found from the lookup

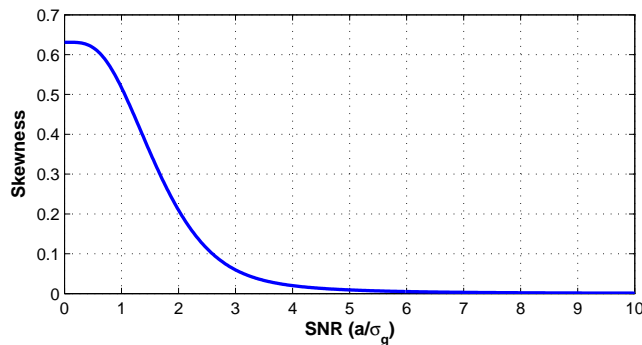


Figure 2.2: Relation between the SNR and skewness for Rician distributed data

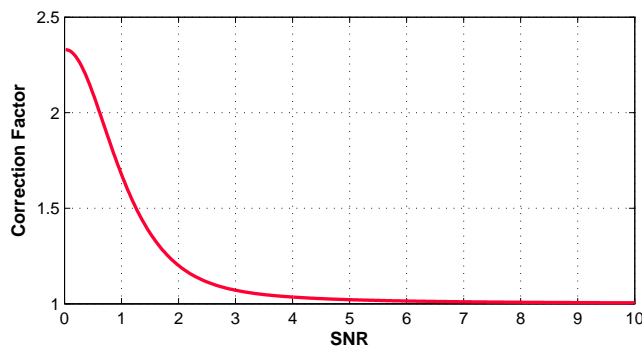


Figure 2.3: Relation between the SNR and correction factor for Rician distributed data

table. A polynomial equation which is an approximation of the look up table is given below

$$\varphi(\mathcal{S}) = \sum_{i=0}^9 p_i \mathcal{S}^i \quad (2.17)$$

The values for the coefficients (with 95% confidence interval) are given in Table 1.

Now, to compute the noise variance in an MR image, the skewness ( $\mathcal{S}$ ) and variance ( $\sigma_r^2$ ) are computed locally for each pixel  $i$ . The correction factor for each pixel can then be found from the lookup table and the corresponding noise variance for each pixel is estimated using Eq. (2.14). Following a similar reasoning as in the previous section, the noise variance can now be estimated as the mode of all local estimates of noise variance around each pixel, which

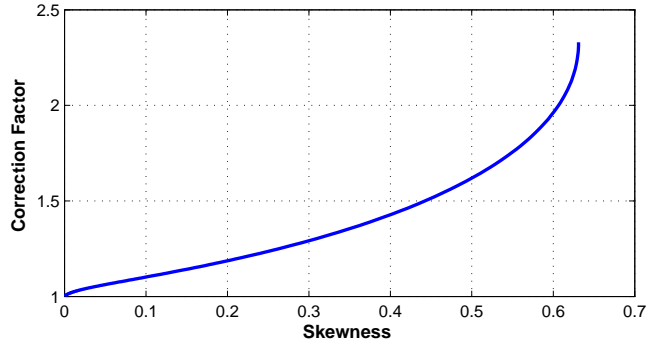


Figure 2.4: Relation between the skewness and variance correction factor for Rician distributed data

can be written as

$$\hat{\sigma}_s^2 = \text{mode}\{\hat{\sigma}_{L(i)}^2\} \quad (2.18)$$

where  $\hat{\sigma}_s^2$  is the estimate of the noise variance in the image and  $\hat{\sigma}_{L(i)}^2$  is the estimated noise variance for a neighborhood around pixel  $i$ .

Table 2.1: Values of the coefficients in Eq. (2.17)

Coefficient	Values
$p_0$	1.00075704
$p_1$	2.8981188340
$p_2$	$7.29432278777 \times 10^1$
$p_3$	$1.1626792136360 \times 10^3$
$p_4$	$-9.83885598962208 \times 10^3$
$p_5$	$4.78139607638493 \times 10^4$
$p_6$	$-1.374485785417688 \times 10^5$
$p_7$	$2.306704056296062 \times 10^5$
$p_8$	$-2.0866638136498138 \times 10^5$
$p_9$	$7.85625551923769 \times 10^4$

## 2.3 Experimental Results

Experiments were conducted on both real and synthetic MR images with and without background region. The window size used in our experiments for local estimates were  $9 \times 9$ . For simulations we used the standard MR image phantom of the brain obtained from the Brainweb database [20] and a cardiac MR image, both with intensity values in the range 0-255. The cardiac image, in contrast to the brain image, contained no background areas. Both images were artificially corrupted with Rician noise with noise level  $\sigma_g$  as 50. Fig. 2.5 shows the distribution of the local estimates of  $\sigma_g$  computed using ML and skewness based methods for both the brain and the cardiac images. It can be observed from the distributions that their mode is almost equal to the true standard deviation of the noise. This experiment demonstrates the independency of the proposed estimators to the image background.

Now, to show the the reliability of the proposed methods in estimating the noise level at both low and high SNR, we conducted the experiments on the cardiac MR image after corrupting the image with Rician noise with  $\sigma_g$  varying from 10 to 100. Results of this experiment are shown in Fig. 2.6. The mean of 100 experiments divided by the actual value of  $\sigma_g$  is depicted. The value closer to 1 is the best estimate. The results are compared with the estimator given in Eq. (2.3). Since, at high SNR the Rician PDF approaches a Gaussian PDF, the estimation based on Eq. (2.3) will be closer to the true  $\sigma_g$ . However, as SNR drops, as expected, it can be seen from the figure that the Gaussian assumption introduces a bias. It can also be observed from the graph that the proposed estimators are significantly less biased. The estimator based on the local ML estimation of  $\sigma_g$  is more close to the true  $\sigma_g$  than the one based on the skewness. However, the time complexity of the skewness based method is less than that of the ML based method. The graph in Fig. 2.7 shows the elapsed time for noise estimation with ML and skewness based methods for image size varying from  $50 \times 50$  to  $300 \times 300$ . In Fig. 2.8 and in Fig. 2.9, the accuracy and precision of the proposed ML based and skewness based estimators for various window (sample) size is depicted.

For the experiments on real data we used the MR image of a cherry

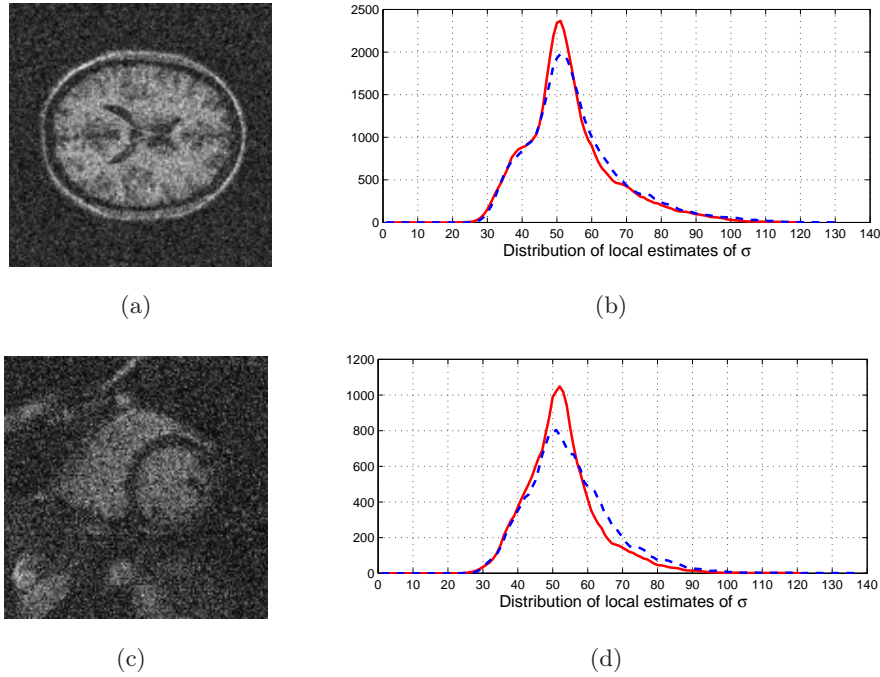


Figure 2.5: Noisy MR images of the brain (a) and heart (b), both corrupted with Rician noise with  $\sigma_g = 50$ . On the right, the distribution of local estimates of  $\sigma_g$  computed using both ML (solid red line) and skewness based methods (dashed blue line) are shown for both the brain (c) and the cardiac (d) images.

tomato (with a mean intensity of around 10,000). A set of MR images was reconstructed by averaging 1 to 12 images. Images reconstructed with 1, 6 and 12 averages are shown in Fig. 2.10. Averaging was done in the complex  $k$ -space. The resulting noise variance as a function of the number of averages over  $n$  images was then estimated. The theoretical reduction of the noise standard deviation as a function of the number of images  $n$  over which the average is taken, is known to be  $1/\sqrt{n}$ . Since the experimental setup for all acquisitions were identical except for averaging, the estimated noise standard deviation  $\hat{\sigma}_g$  multiplied by  $\sqrt{n}$  is expected to be constant as a function of  $n$ . It can be seen from Fig. 2.11 that the proposed methods exhibits this property.

### 2.3. Experimental Results

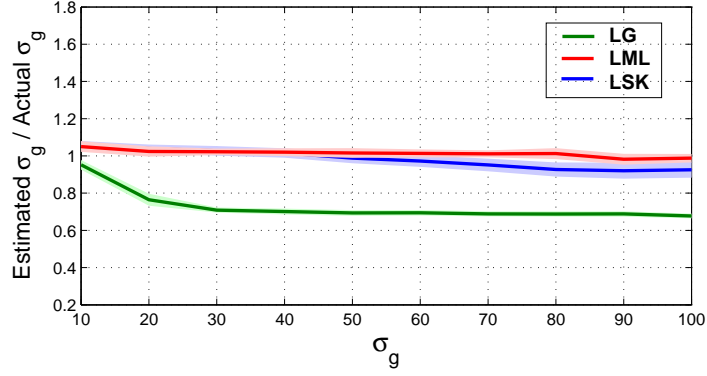


Figure 2.6: The estimated  $\sigma_g$  / actual  $\sigma_g$  for various values of  $\sigma_g$  ranging from 10 to 100. This experiment was done on the Cardiac MR image. The red and blue line corresponds to the proposed methods using ML and skewness, respectively, and the green line corresponds to the estimator given in Eq. (2.3). The shaded area shows the standard deviation for 100 experiments.

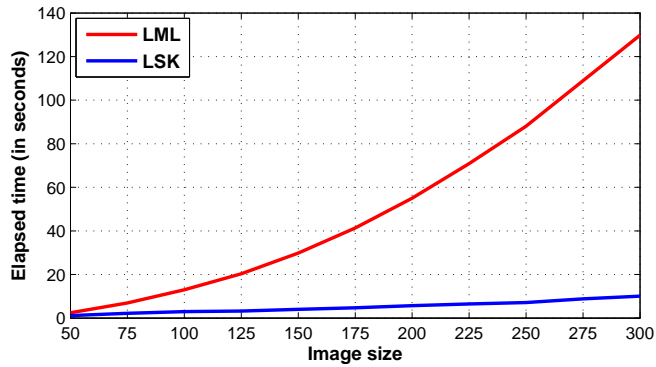


Figure 2.7: Elapsed time for noise estimation with ML and skewness based methods for image size varying from  $50 \times 50$  to  $300 \times 300$ .

## 2.3. Experimental Results

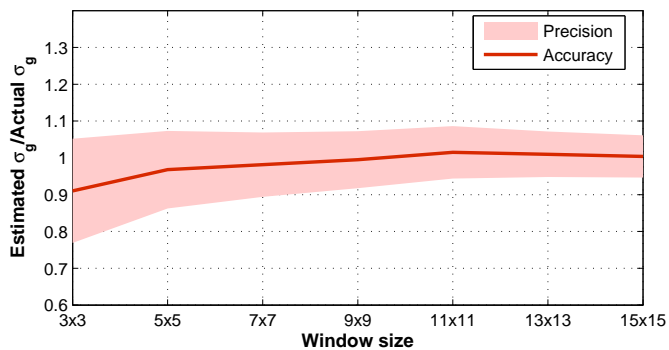


Figure 2.8: Precision and accuracy of the proposed ML based estimator for different window size.

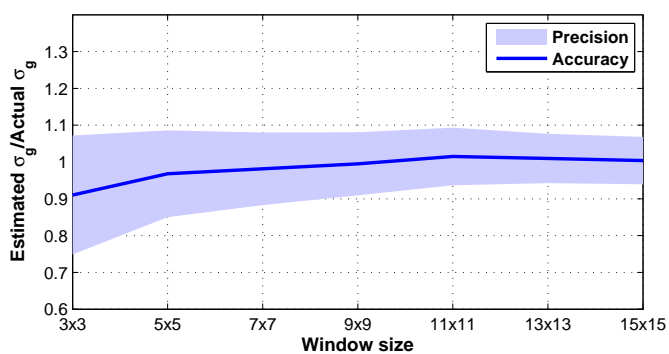


Figure 2.9: Precision and accuracy of the proposed skewness based estimator for different window size.

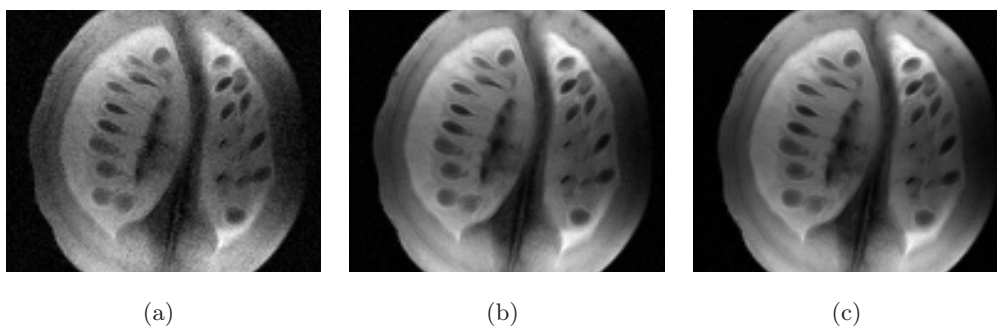


Figure 2.10: MR images of cherry tomato (a) acquired without averaging (b) acquired with 6 averages (c) acquired with 12 averages.

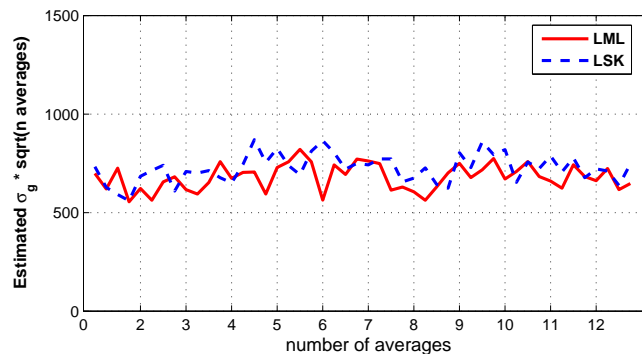


Figure 2.11: Estimated  $\sigma_g$  as a function of the number of averages  $n$  used during the acquisition. MR image of a cherry tomato was used for this experiment.

## 2.4 Conclusion

Two different approaches based on the local estimates of the variance and skewness were proposed to address the estimation of the noise from MR images when the Rayleigh background data or high SNR image regions are not available. The estimation of  $\sigma_g$  based on local ML is slightly more accurate than the method based on the skewness. However, the time complexity of the ML based method is significantly larger than that of the skewness based method. Experimental results on synthetic and real MR images show the reliability of the proposed methods. Even though the proposed methods are based on the noise characteristics of magnitude image data acquired with single coil MRI, it can, under certain conditions, be extended for multiple coil imaging methods.

### References

- [1] R. D. Nowak, “Wavelet based Rician noise removal for magnetic resonance images,” *IEEE Trans. Image Processing*, vol. 10, no. 8, pp. 1408–1419, 1999.
- [2] J. Sijbers, A. J. den Dekker, A. Van der Linden, M. Verhoye, and D. Van Dyck, “Adaptive anisotropic noise filtering for magnitude MR data,” *Magn Reson Imaging*, vol. 17, no. 10, pp. 1533–1539, 1999.

- [3] S. Basu, T. Fletcher, and R. Whitaker, “Rician noise removal in diffusion tensor MRI,” in *Medical Image Computing and Computer-Assisted Intervention - MICCAI 2006*, Berlin, 2006, pp. 117–125, Springer-Verlag.
- [4] S. Aja-Fernández, C. Alberola-López, and C.F. Westin, “Noise and signal estimation in magnitude MRI and rician distributed images: a LMMSE approach,” *IEEE Trans Imag Proc*, vol. 17, pp. 1383–1398, 2008.
- [5] Ranjan Maitra and David Faden, “Noise estimation in magnitude MR datasets,” *IEEE Trans. on Medical Imaging*, vol. 28, pp. 1615–1622, 2009.
- [6] J. Sijbers, A. J. den Dekker, M. Verhoye, J. Van Audekerke, and D. Van Dyck, “Estimation of noise from magnitude MR images,” *Magn Reson Imaging*, vol. 16, no. 1, pp. 87–90, 1998.
- [7] J. T. Heverhagen, “noise measurement and estimation in MR imaging experiments,” *Radiology*, vol. 245, pp. 638–639, 2007.
- [8] M. E. Brummer, R. M. Mersereau, R.L. Eisner, and R.R.J. Lewine, “Automatic detection of brain contours in MRI data sets,” *IEEE Trans Med Imaging*, vol. 12, no. 2, pp. 153–168, 1993.
- [9] J. Sijbers and A. J. den Dekker, “Maximum likelihood estimation of signal amplitude and noise variance from MR data,” *Magn Reson Med*, vol. 51, no. 3, pp. 586–594, 2004.
- [10] J. Sijbers, D. Poot, A. J. den Dekker, and W. Pintjens, “Automatic estimation of the noise variance from the histogram of a magnetic resonance image,” *Phys Med Biol*, vol. 52, pp. 1335–1348, 2007.
- [11] S. Aja-Fernández, A. Tristán, and C. Alberola-López, “Noise estimation in single and multiple coil magnetic resonance data based on statistical models,” *Magn Reson Imaging*, vol. 27, pp. 1397–1409, 2009.
- [12] R. M. Henkelman, “Measurement of signal intensities in the presence of noise in MR images,” *Med Phys*, vol. 12, no. 2, pp. 232–233, 1985.

- [13] S. Aja-Fernández, G. Vegas-Sánchez-Ferrero, and A. Tristán-Vega, “About the background distribution in MR data: a local variance study,” *Magn Reson Imaging*, vol. 28, pp. 739–752, 2010.
- [14] J. Sijbers, A. J. den Dekker, P. Scheunders, and D. Van Dyck, “Maximum likelihood estimation of Rician distribution parameters,” *IEEE Trans. Med. Imag.*, vol. 17, no. 3, pp. 357–361, June 1998.
- [15] J. Rajan, D. Poot, J. Juntu, and J. Sijbers, “Segmentation based noise variance estimation from background mri data,” in *Proceedings of the 7th international conference on Image Analysis and Recognition*. 2010, pp. 32–70, LNCS, Springer-Verlag.
- [16] G.M.P. van Kempen and L.J. van Vliet, “The influence of the background estimation on the superresolution properties of non-linear image restoration algorithms,” in *Three-Dimensional and Multidimensional Microscopy: Image Acquisition and Processing VI: Proceedings of SPIE Progress in Biomedical Optics*, D. Cabib, C.J. Cogswell, J.A. Conchello, J.M. Lerner, and T. Wilson, Eds., 1999, vol. 3605, pp. 179–189.
- [17] Lin-Ching Chang, Gustavo K. Rohde, and Carlo Pierpaoli, “An automatic method for estimating noise-induced signal variance in magnitude-reconstructed magnetic resonance images,” in *SPIE Medical Imaging 2005: Image Processing*, April 2005, vol. 5747, pp. 1136–1142.
- [18] Y. Zhang, M. Brady, and S. Smith, “Segmentation of brain mr images through a hidden markov random field model and the expectation maximization algorithm,” *IEEE Trans Med Imaging*, vol. 20, no. 1, pp. 45–57, 2001.
- [19] C G Koay and P J Basser, “Analytically exact correction scheme for signal extraction from noisy magnitude MR signals,” *Journal of Magnetic Resonance*, vol. 179, pp. 317–322, 2006.
- [20] C. A. Cocosco, V. Kollokian, R.K.-S. Kwan, and A. C. Evans, “Brainweb: Online interface to a 3D MRI simulated brain database;

<http://www.bic.mni.mcgill.ca/brainweb/>," *NeuroImage*, vol. 5, no. 4, pp. S425, 1997.

# Maximum likelihood estimation based denoising of MR Images

---

## Contents

---

<b>3.1</b>	<b>Introduction</b>	<b>42</b>
<b>3.2</b>	<b>Methods</b>	<b>44</b>
3.2.1	Signal estimation using LML	44
3.2.2	Non local means algorithm	45
3.2.3	Signal estimation using restricted LML	47
3.2.4	Spatially varying noise levels	48
<b>3.3</b>	<b>Experiments and Results</b>	<b>49</b>
<b>3.4</b>	<b>Conclusion</b>	<b>57</b>

---

The work described in this chapter has been published as:

**J. Rajan**, B. Jeurissen, M. Verhoye, J. Van Audekerke and J. Sijbers, “Maximum likelihood estimation based denoising of magnetic resonance images using restricted local neighborhoods”, *Physics in Medicine and Biology*, vol 56, pp 5221- 5234, 2011

### Abstract:

In this chapter, we will discuss a method that we proposed to denoise magnitude MR images, which are Rician distributed. Conventionally, ML

methods incorporate the Rice distribution to estimate the true, underlying signal from a local neighborhood within which the signal is assumed to be constant. However, if this assumption is not met, such filtering will lead to blurred edges and loss of fine structures. As a solution to this problem, we put forward the concept of restricted local neighborhoods where the true intensity for each noisy pixel is estimated from a set of preselected neighboring pixels. To this end, a reference image is created from the noisy image using a recently proposed non local means algorithm. This reference image is used as a prior for further noise reduction. A scheme is developed to locally select an appropriate subset of pixels from which the underlying signal is estimated.

### 3.1 Introduction

As discussed in chapters 1 and 2, the data acquired by an MRI system are inherently corrupted by noise which has its origin in the thermal Brownian motion of electrons. Noise remains one of the main causes of quality deterioration in MRI and is a subject in a large number of papers in MRI literature, e.g [1, 2, 3, 4, 5, 6]. Other than visual analysis, processing techniques such as segmentation, registration or tensor estimation in diffusion tensor MRI (DT-MRI) will be affected or biased due to noise [7, 8].

Noise can be naturally minimized by averaging images after multiple acquisitions. This, however, may not be feasible in clinical and small animal MR imaging where there is an increasing need for speed [9]. Thus, post processing techniques to remove noise in the acquired data are important. Also, time-sensitive acquisitions in contrast material-enhanced studies, functional studies, diffusion MRI (dMRI) or studies with limited imaging time, experiments cannot be repeated to do averaging.

Several filtering techniques to improve the quality of the MR images have been proposed in the literature. Most of the methods proposed earlier can be mainly classified as either based on Partial Differential Equations (PDEs), wavelets or Non Local Means (NLM). A PDE based approach for filtering MRI was first attempted by Gerig et al. [10]. In their work, they demonstrated that anisotropic diffusion is an effective filtering technique for MRI in the sense that

it can significantly decrease the image noise and simultaneously preserve fine details in the image. A major drawback of their method, however, was the incorrect assumption about the noise distribution. The noise was assumed to be Gaussian instead of Rician, as a result of which a bias is introduced in the filtered image. Such a bias becomes particularly important in low SNR MR images, such as diffusion weighted images [11]. To account for the Rice distribution, an adaptive anisotropic diffusion method for magnitude MR data was proposed by Sijbers et al. [12]. Finally, Samsonov and Johnson [13], presented a noise adaptive nonlinear diffusion filtering technique to denoise MR images with spatially varying noise levels.

All aforementioned PDE methods are based on classical  $2^{nd}$  order Perona-Malik [14] anisotropic diffusion. Although such methods are effective in denoising images, they tend to cause staircase effects in the filtered images [15]. To reduce this effect, a noise removal algorithm for MRI based on fourth order PDE was suggested by Lysaker et al. [16]. The main strength of this method is its ability to process signals with a smooth change in the intensity value. Basu et al. [17] used a data likelihood term combined with Perona-Malik anisotropic diffusion to effectively denoise an MR image. Recently Krissian and Aja-Fernández [18] proposed a noise driven anisotropic diffusion filter for denoising MR images, in which the diffusion is controlled by the local statistics in the image derived from the linear minimum mean square error (LMMSE) estimator for the Rician model.

A second class of noise filtering schemes are wavelet based [19, 20, 21]. These algorithms exploit the decorrelating properties of the wavelet transform to suppress noise coefficients using statistical inference. Among these methods, [19] got much attention, in which a bias removal was proposed, based on the observation that the squared Rician distributed data exhibits a chi-squared distribution with two degrees of freedom. However, in [9], it is mentioned that the aforementioned wavelet based filters may introduce characteristic artifacts that can be quite problematic. A trilateral filter was proposed in [22] to take into account the local structure in the image, in addition to intensity and geometric features. Recently Delakis et al. [23] proposed a wavelet based denoising algorithm for images acquired with parallel MRI.

During the past years, NLM based denoising methods gained much popularity [24]. Manjón et al. [9] were the first to attempt MRI denoising with the NLM approach. Coupé et al. [25] proposed an optimized blockwise version of the NLM algorithm for denoising MR images. Wiest-Daesslé et al. [26] suggested an adaptive NLM filter which behave better for Rician corrupted MR data. Aja-Fernández et al. [27] incorporated the LMMSE approach in NLM to make it adaptive for Rician data. Recently, Manjón et al. [28] proposed an adaptive NLM denoising method for MR images with spatially varying noise levels. Apart from the above discussed methods, other popular approaches proposed for MR denoising are the methods based on ML estimation [29, 30] and the filtering based on smoothing splines [31].

In this chapter, we propose a method to denoise magnitude MRI based on the ML estimation method using a restricted local neighborhood. ML estimation can be applied locally (also referred as local ML(LML)) or non locally as proposed by He and Greenshields [30], in which ML estimation is applied on a set of pixels selected based on the similarity of the neighborhood. One drawback of the non local ML (NLML) estimation method is the use of a fixed sample size for the ML estimation, which causes either under or over smoothing. The disadvantage of the LML method is the blurring of edges and the distortion of fine structures in the image. This is because the assumption that the signal in the selected small neighborhood is constant, is generally not valid. In this chapter, we put forward the concept of a restricted local neighborhood as a solution to this problem.

## 3.2 Methods

### 3.2.1 Signal estimation using LML

As discussed in Chapter 2, the ML estimator of underlying true intensity  $a$  from a set of magnitude observations  $\{m_i\}$  can be defined as an estimator maximizing the log likelihood function:

$$\ln \mathcal{L} = \sum_{i=1}^n \ln \left( \frac{m_i}{\sigma_g^2} \right) - \sum_{i=1}^n \frac{m_i^2 + a^2}{2\sigma_g^2} + \sum_{i=1}^n \ln I_0 \left( \frac{am_i}{\sigma_g^2} \right) \quad (3.1)$$

and

$$\hat{a}_{\text{ML}} = \arg\{\max_a(\ln \mathcal{L})\} \quad (3.2)$$

where  $a_{\text{ML}}$  is the estimated true intensity and  $\sigma_g^2$  in Eq. (3.1) is the noise variance in the complex image, which can be estimated using the methods explained in the previous chapter.

The straightforward approach to denoise MR images using the ML estimation method in Eq. (3.2) is to apply the method locally for each pixel with the assumption that the underlying area is constant for a local region. However, this assumption is not valid for regions with edges and fine structures and as a result these regions will get blurred. The effects of applying local ML (LML) on a noisy image can be observed from Fig. 3.1. It can also be observed from Fig. 3.1(c) and Fig. 3.1(d) that the image denoised with a window size of  $3 \times 3 \times 3$  is, not surprisingly, less blurred than the one denoised with a window size of  $5 \times 5 \times 3$ . However, selecting a very small window size is less effective for denoising, especially in smooth areas, since the number of samples for estimation is smaller.

In the proposed method, we consider only the pixels that have an underlying gray level value close to that of the center pixel in the local window for the true signal estimation, instead of selecting all pixels in the window. This approach can reduce the side effects of LML estimation. However, selection of pixels with similar underlying gray value from a noisy image is a difficult problem. To solve this issue, we used a reference image. The reference image is created by applying the NLM algorithm over the noisy image. Based on the information from the reference image, corresponding pixels are selected from the noisy image for true signal estimation.

### 3.2.2 Non local means algorithm

The NLM method which we used to create the reference image is briefly explained in this section. The NLM method was proposed by Buades et al [24] and is based on the Markovian hypothesis which states that pixels with a similar neighborhood have a similar gray level value. Given a noisy image  $M = \{m_i | i \in \Omega\}$ , where  $\Omega$  represents the image space and  $m_i$  corresponds to

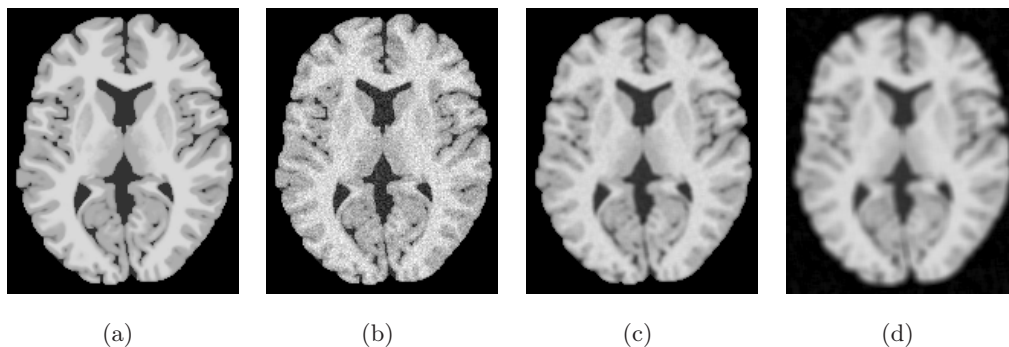


Figure 3.1: Denoising MRI with LML method (a) Original image (b) Original image corrupted with Rician noise of  $\sigma_g = 15$ . (c) Noisy image denoised with LML of window size  $3 \times 3 \times 3$  (d) Noisy image denoised with LML of window size  $5 \times 5 \times 3$ . The blurring effect generated by the LML method can be observed from the denoised images.

the noisy image value at location  $i$ , then the filtered value at a point  $i$ ,  $r_i$ , is calculated using the NLM method as a weighted average of all the pixels in the image [24]:

$$r_i = \frac{1}{c_i} \sum_{j \in \Omega_s} w_{i,j} m_j, \quad (3.3)$$

where  $\Omega_s$  represents the neighborhood pixels and

$$c_i = \sum_{j \in \Omega_s} w_{i,j} \quad (3.4)$$

is a normalization constant and the weight  $w_{i,j}$  is determined by the similarity of the Gaussian neighborhood between pixels  $i$  and  $j$ , which can be expressed as:

$$w_{i,j} = \exp\left(-\frac{\|N_i - N_j\|_{2,u}^2}{h^2}\right) \quad (3.5)$$

where  $N_i$  denotes a square neighborhood centered at pixel  $i$ ,  $\|\cdot\|_{2,u}^2$  is a Gaussian weighted Euclidean distance function,  $u$  is the standard deviation of the Gaussian kernel and  $h$  acts as a degree of filtering.

### 3.2.3 Signal estimation using restricted LML

To overcome the drawback of the LML estimation method, we propose a restricted LML (RLML) estimation method. In RLML, only the pixels in the local neighborhood of the noisy pixel  $m_i$  that have an underlying gray level value close to the underlying gray level value of  $m_i$ , will be considered for the true signal estimation. However, as mentioned earlier, selection of pixels with similar underlying gray value from a noisy image is a difficult problem. To this end, we create a reference image using the above mentioned NLM method. Now, to denoise a noisy pixel  $m_i$  at  $i$ , a list  $l_i$  is created from the neighbors of  $m_i$ :

$$l_i = \{m_j, (j \in \Omega_m) \mid \text{abs}(f(m_j) - f(m_i)) < t\} \quad (3.6)$$

where  $\Omega_m$  represents the neighborhood space around  $m_j$ ,  $f(m_j) = r_j$  and  $f(m_i) = r_i$ . The threshold  $t$  used for the classification is calculated from the reference image as the range of the intensity dispersion of a uniform area. This can also be automatically computed from the reference image,  $R$ , as the mode of all the local distributions of the range computed around the neighborhood of each pixel:

$$t = \text{mode}\{\text{range}(R_F)_w\} \quad (3.7)$$

where  $R_F$  represents the foreground region of the reference image and  $w$  is the neighborhood window size. Contrary to complex valued images, where the noise is Gaussian distributed, in magnitude images the range of intensity dispersion has a dependency on the local SNR due to the non linear operation used to create the magnitude images. Hence, to reduce the error in the classification of pixels in the reference image, the threshold  $t$  is computed only from the foreground region of the image. Fig. 3.2 shows the distribution of the local range for a uniform region in the reference image and also the distribution of the local range computed with a neighborhood size of  $3 \times 3$  and  $5 \times 5$ . It can be observed from the plots in the figure that the mode of the distributions of the local range is close to the actual range of the intensity dispersion of the selected homogeneous region. Once a list is created as mentioned in Eq. (3.6), the denoised pixel  $\hat{a}_i$  at location  $i$  can be computed by substituting the values in the list  $l_i$  as the Rician distributed magnitude data points in Eq. (3.1)

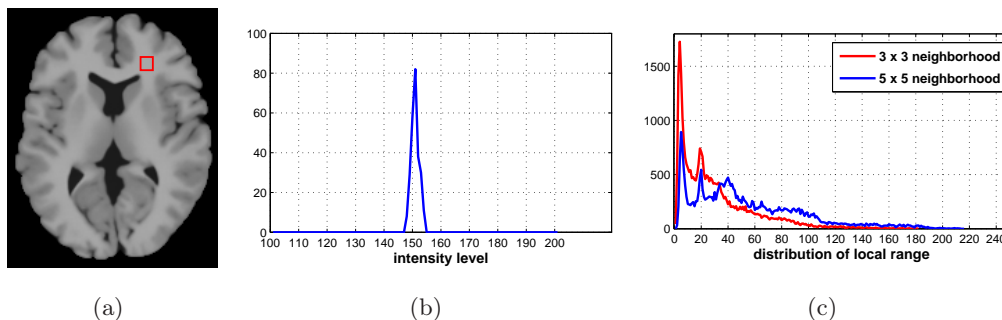


Figure 3.2: Computation of threshold from ROI and from the mode of the local distribution of range (a) Reference image with ROI (marked as red) (b) distribution of intensity in the ROI (c) distribution of local range computed using  $3 \times 3$  and  $5 \times 5$  neighborhood.

and then maximizing the log likelihood function. Applying this procedure to all pixels in the noisy image will give the denoised image. The method is summarized in Algorithm 1.

---

**Algorithm 1** Algorithm for signal estimation using RLML

---

- 1: Estimate the noise standard deviation  $\sigma_g$  from the input magnitude image  $M$  using the method described in [32].
  - 2: Create the reference image  $R$  using Eq. (3.3)
  - 3: Compute the threshold  $t$  from  $R$  by applying Eq. (3.7) using a neighborhood window of size  $n \times n \times n$
  - 4: **for** every pixel  $m_i$  of  $M$  **do**
  - 5:   Create the list  $l_i$  as mentioned in Eq. (3.6) using a neighborhood window of size  $w \times w \times w$
  - 6:   Substitute the values in the list  $l_i$  in Eq. (3.1)
  - 7:   Estimate  $\hat{a}_i$  by maximizing Eq. (3.1) with respect to the unknown true intensity.
- 

### 3.2.4 Spatially varying noise levels

Once we know  $\sigma_g$  and the samples  $l_i$  we can compute the underlying true intensity using the above mentioned procedure. When measuring the noise in MR images, it is often assumed that the noise level  $\sigma_g$  is the same across the

image. However this is not always the case. Parallel MRI (pMRI) acquisition techniques such as sensitivity encoding (SENSE) introduces spatially varying noise in the image when the  $k$ -space is subsampled to decrease the acquisition time [33, 28, 8].

When dealing with images with spatially varying noise, the noise map  $\sigma_s$  should be used instead of  $\sigma_g$  to get optimal results with the proposed method. The noise map  $\sigma_s$  in a SENSE reconstructed image depends on the geometry factor  $g$  and the reduction factor  $R$  and is given by [33]:

$$\sigma_s = g\sqrt{R}\sigma_f \quad (3.8)$$

where  $\sigma_f$  is the noise level in the fully sampled  $k$ -space.

However, in the absence of such a noise map (if only magnitude image is available), both underlying intensity and the noise variance can be estimated simultaneously from the samples  $l_i$  by maximizing the log likelihood function in Eq. (3.1) with the assumption that the noise level is same in a small enough local region. The ML estimate is then found from the global maximum of  $\ln \mathcal{L}$  w.r.t.  $a$  and  $\sigma_s^2$  [29]:

$$\{\hat{a}_{\text{ML}}, \hat{\sigma}_{s\text{ML}}^2\} = \arg\{\max_{a, \sigma_s^2}(\ln \mathcal{L})\} \quad (3.9)$$

### 3.3 Experiments and Results

To evaluate and compare the proposed method with the state-of-the-art methods, we did experiments on both synthetic and real MR images. To conduct the experiments on synthetic data, we used the standard MR image phantom of the brain obtained from the Brainweb database [34] (T1-weighted, intensity values in the range 0-255) and for the experiments on DWI, we simulated a set of DWI of the human brain using the methods in [35, 36]. For the experiments on real data, we used the MR images of a Kiwi fruit. The proposed algorithm was compared with the following recently proposed methods.

1. NLML: The non local maximum likelihood method [30] with search window size =  $11 \times 11 \times 11$ , neighborhood size =  $3 \times 3 \times 3$ , and sample size 25.

2. UNLM: Unbiased non local means [9] with search window size =  $11 \times 11 \times 11$ , neighborhood size =  $3 \times 3 \times 3$ , value of the decay parameter  $h = \sigma_g$ .
3. RNRAD: Noise driven anisotropic diffusion filter for MRI [18]. Local statistics were computed on a  $3 \times 3 \times 3$  neighborhood and time step as  $dt = 1/6$ . For simulations, the number of iterations was chosen as the one with best PSNR when compared with the original image.
4. ARNLM: Adaptive Rician non local means filter with wavelet mixing [28].

For quantitative analysis of the denoising methods we used the Peak Signal to Noise Ratio (PSNR), the Structural Similarity Index Matrix (SSIM)[37], Bhattacharyya coefficient (BC)[38] and the Mean Absolute Difference (MAD).

Fig. 3.3 shows the visual quality comparison of the image denoised with NLML, UNLM, RNRAD and the proposed RLML method. This experiment was conducted on a 2D slice of the synthetic image of the brain in the 3D environment after corrupting the image by noise with  $\sigma_g = 20$ . The proposed RLML filter was executed with the following parameters: neighborhood size for denoising as  $7 \times 7 \times 3$  and the neighborhood size for the local computation of the range as  $3 \times 3 \times 3$ .

In visual analysis, the expectations are (i) perceptually flat regions should be smooth as possible (ii) image edges and corners should be well preserved (iii) texture detail should not be lost and (iv) few or ideally no artifacts [30, 39]. It can be observed from Fig. 3.3 that the image denoised with the proposed method is closer to the original one (based on the above mentioned criteria) than the images denoised with the other approaches. Also the comparison of the histograms of the simulated true image and the denoised images displayed in Fig. 3.4 shows that the image denoised with the proposed method is more close to the ground truth than other images. Fig. 3.5 shows the quantitative analysis of the proposed method with other recently proposed methods. All the methods to which the proposed method was compared were based on the Rician noise model. In the quantitative analysis, the background was

excluded; that is, only the area of the image inside the skull was considered. It can be studied from the plots in Fig. 3.5 (taken as a mean of 15 experiments) that the proposed method outperforms other approaches in terms of PSNR, SSIM, BC and MAD.

Fig. 3.6 and Fig. 3.8 show the results of the experiment conducted on the synthetic image of the brain with spatially varying noise which was generated using the method mentioned in [28]. The noisy images are then denoised with the proposed RLML and also with the recently proposed ARNLM filter. Since the NLM approach is not effective in case of spatially varying noise, we used the adaptive NLM (ANLM) proposed in [28] as the reference image for threshold computation. Both visual and quantitative analysis show that the image processed with RLML is more effective than ARNLM in denoising spatially varying noise.

Fig. 3.7 shows the experiments on the synthetic image reconstructed with SENSE method with an acceleration factor of 2. This experiment was conducted on the standard Brainweb test image by multiplying the test image with 4 different coil sensitivities. Noise of  $\sigma_g = 20$  was added to the complex image before creating the reduced FOV images. Four reduced FOV images with a reduction factor of 2 were created. Full FOV complex image was then created from the reduced FOV images using the SENSE reconstruction algorithm. The reconstructed image was then denoised with ARNLM and also with the proposed method .

For the experiments on DW-MRI, we simulated a set of DW images of the human brain with the following parameters:  $b = 1200s/mm^2$ , voxel size =  $1.79 \times 1.79 \times 2.4mm^3$ , image size =  $107 \times 79 \times 60$  and the gradient orientations = 15. The DW images was then corrupted with Rician noise of  $\sigma_g = 100$ . The denoised DW images was then generated using the proposed method and other methods mentioned earlier. The fractional anisotropy (FA) map was calculated for the ground truth, the noisy and the denoised methods (see Fig. 3.9). Fig. 3.10 shows the absolute difference of the estimated FA map with the original FA map for the noisy and all denoising methods. The MAD of the FA residuals shows that the error in the FA map computed from the image denoised with the proposed method is comparatively smaller than the

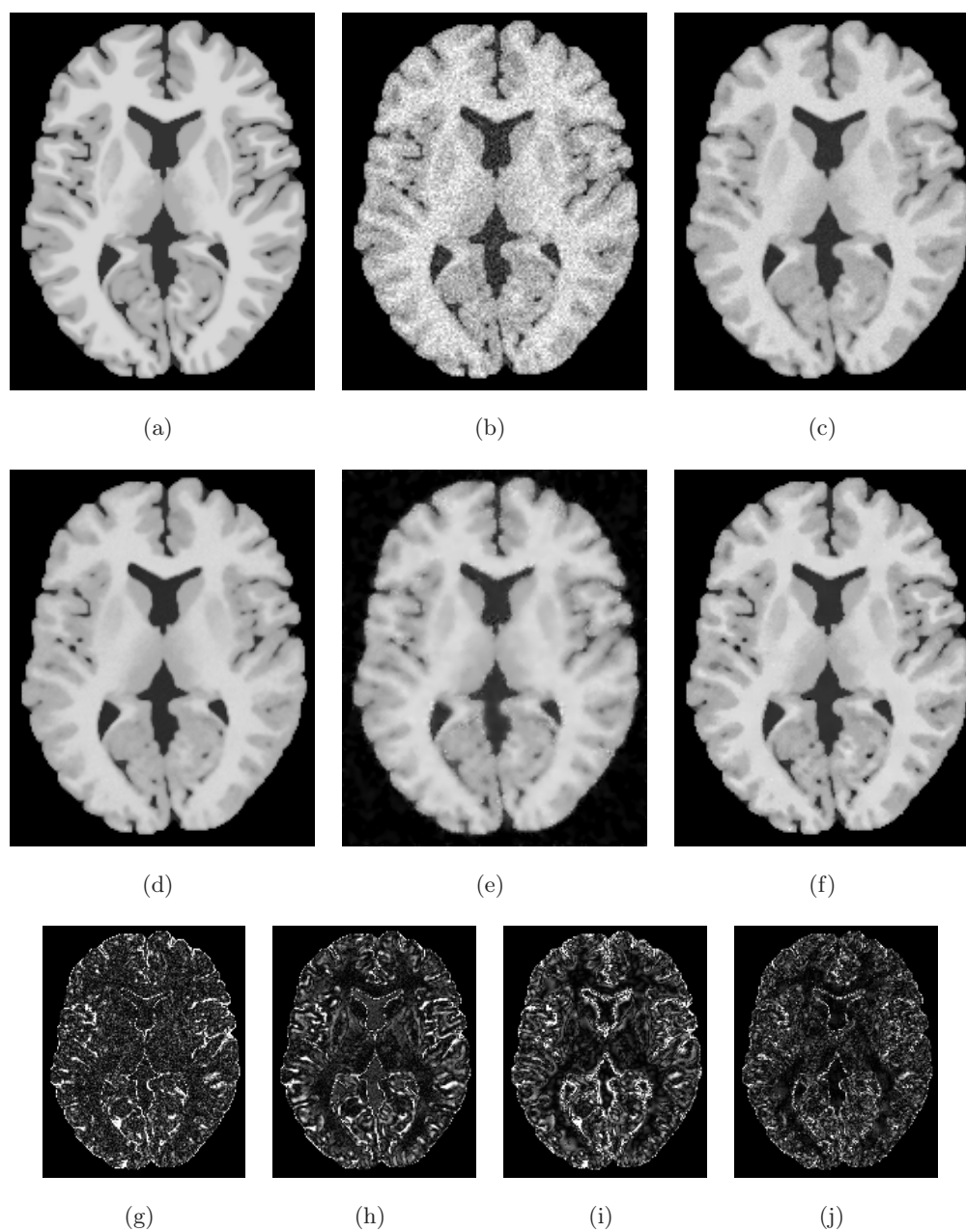


Figure 3.3: Denoising MRI with various methods :**(a)** Original image **(b)** Original image corrupted with Rician noise of  $\sigma_g = 20$  **(c)** (b) denoised with NLML method **(d)** (b) denoised with UNLM method **(e)** (b) denoised with RNRAD method **(f)** (b) denoised with RLML method **(g)**, **(h)**, **(i)**, **(j)** are the residual images (in the range 0 - 25) of **(c)**, **(d)**, **(e)**, **(f)**.

### 3.3. Experiments and Results

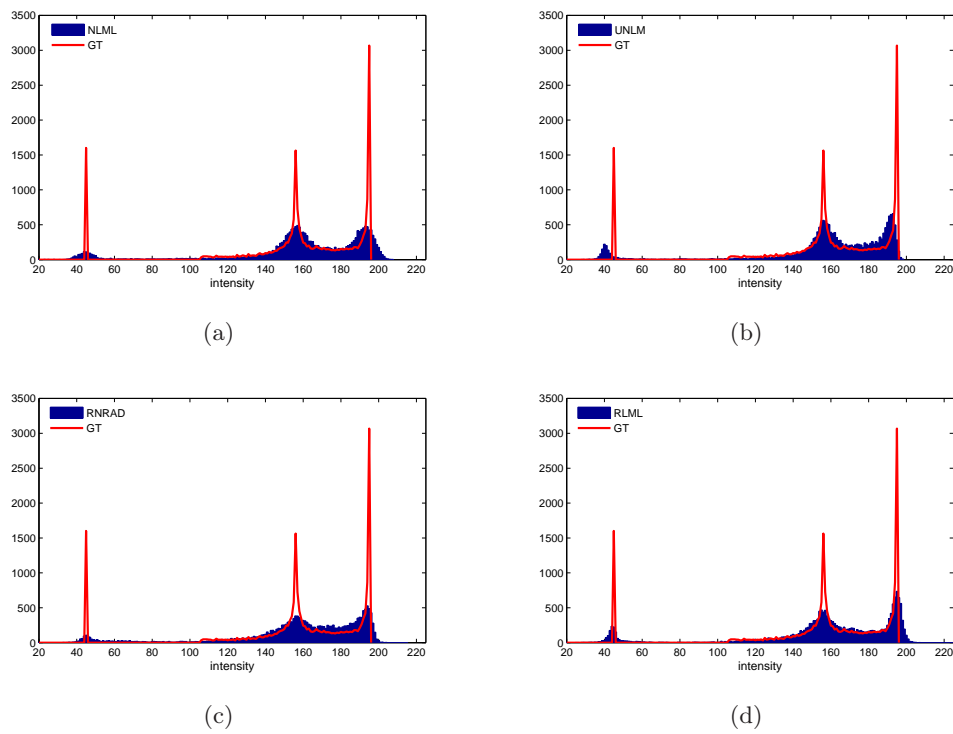


Figure 3.4: Comparison of the histograms of the simulated ground truth (GT) with the histogram of the denoised images (a) with NLML (b) with UNLM (c) with RNRAD (d) with RLML.

### 3.3. Experiments and Results

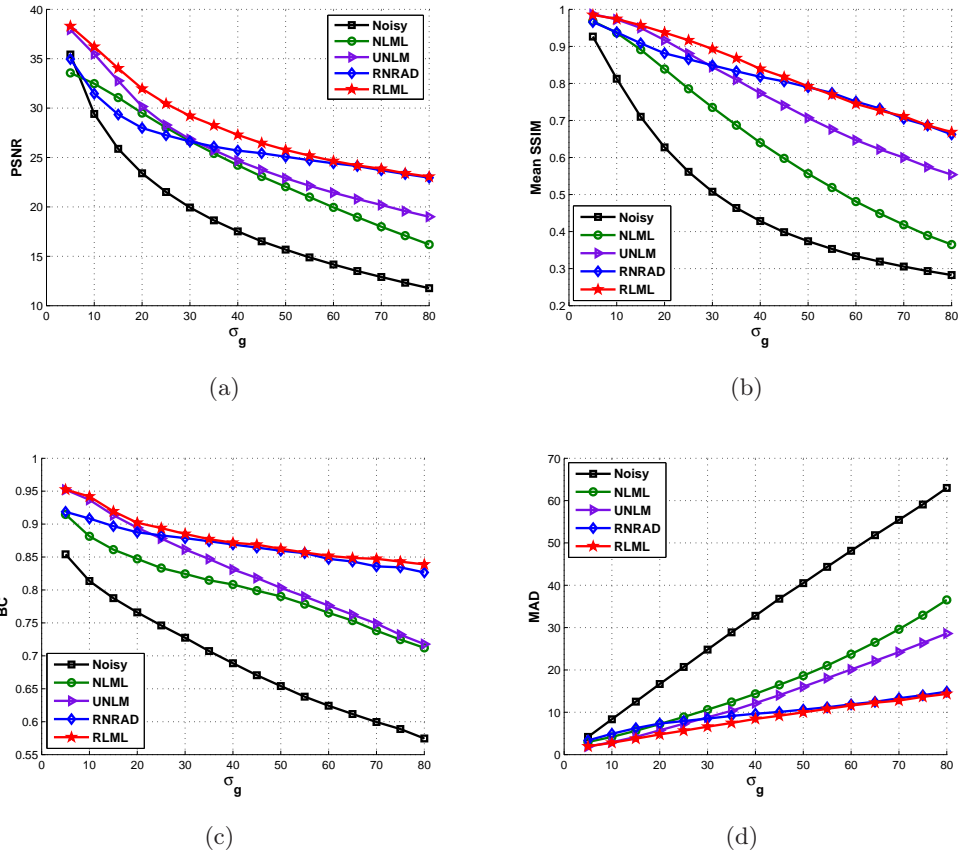


Figure 3.5: Quantitative analysis of the proposed method with other recently proposed methods based on (a) PSNR (b) SSIM (c) BC and (d) MAD for image corrupted with Rician noise of  $\sigma_g$  varying from 5 to 80.

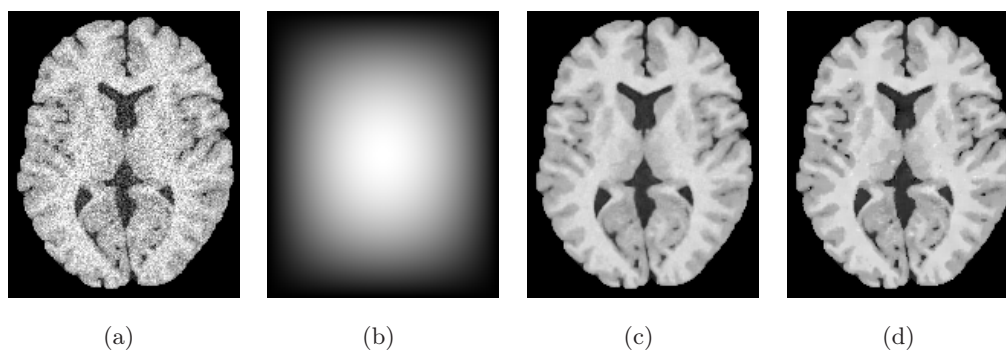


Figure 3.6: Denoising MRI with spatially varying noise levels (a) Noisy image with spatially varying noise (b) noise modulation map (c) noisy image denoised with ARNLM method (d) noisy image denoised with proposed RLML method.

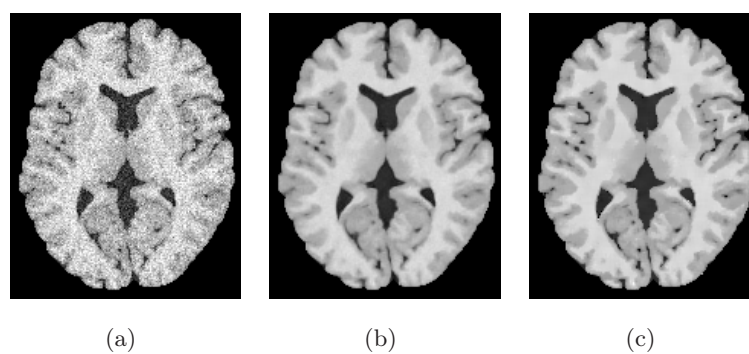


Figure 3.7: Denoising SENSE reconstructed MRI with 4 coils and acceleration factor = 2 (a) Noisy image with spatially varying noise (b) with ARNLM (PSNR : 31.1639) (c) with RLML using Eq. (3.9) PSNR : 31.7544

### 3.3. Experiments and Results

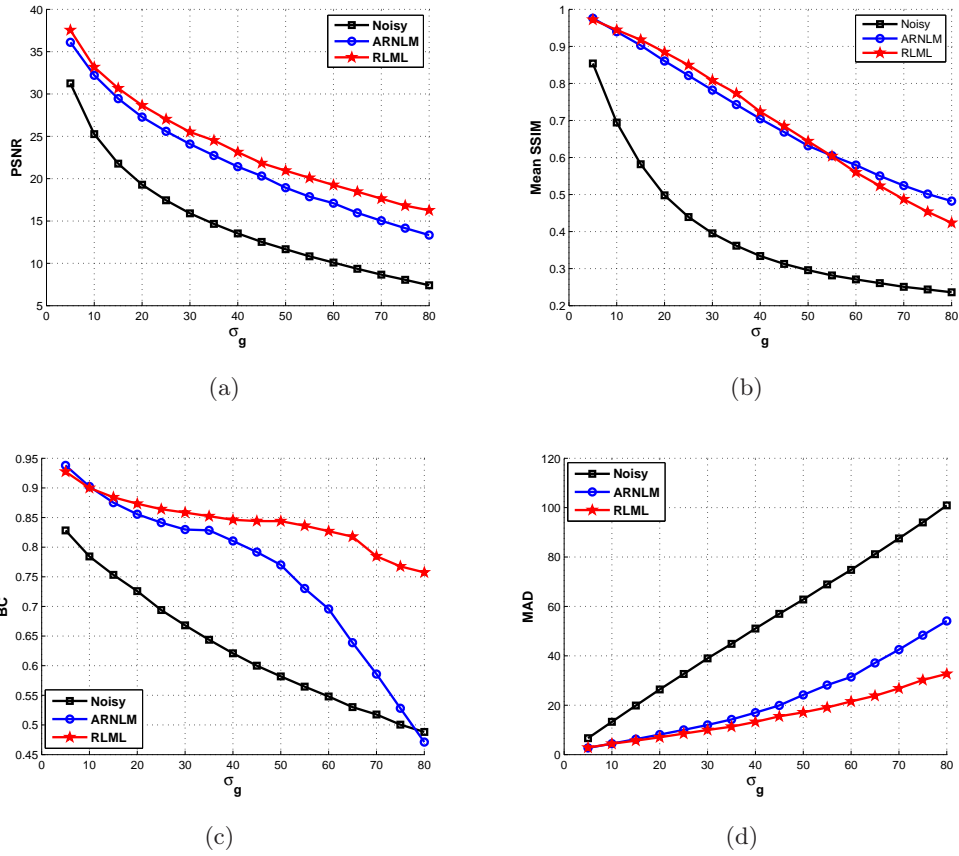


Figure 3.8: Performance comparison of the RLML method against a recently proposed ARNLM method in terms of (a) PSNR (b) SSIM (c) BC and (d) MAD for image corrupted with spatially varying Rician noise of  $\sigma_g$  varying from 5 to 80.

other methods.

Fig. 3.11 shows the results of applying the different denoising methods on an MR image of a kiwi fruit. Two sets of kiwi fruit images were reconstructed, one without averaging and the other by averaging 12 acquisitions. Averaging was done in the complex k-space. The denoising algorithms were then applied over the image reconstructed without averaging and the resultant denoised image was compared with the image reconstructed by averaging 12 acquisitions. It can be observed from the images that the visual results are much better for RLML in terms of image contrast. Quantitative analysis of the experiments on the kiwi fruit was done based on the second order moment of the Rice distribution :

$$E[M^2] = a^2 + 2\sigma_g^2 \quad (3.10)$$

If we assume the denoised image  $\hat{a}$  as the ground truth, then  $\hat{\sigma}_g^2$  can be estimated as

$$\hat{\sigma}_g^2 = \frac{\langle M^2 \rangle - \langle \hat{a}^2 \rangle}{2} \quad (3.11)$$

where  $\langle \rangle$  denotes the spatial average of the whole image. The closer the estimated  $\hat{\sigma}_g^2$  to the actual noise variance, the closer the denoised image  $\hat{a}$  to the ground truth. The result of this experiment is given in Table. 3.1. It is clear from the table that the  $\hat{\sigma}_g$  estimated for the image denoised with the proposed RLML method is more close to the actual noise standard deviation. The estimated standard deviation of the noise from the image acquired without averaging is 27.5. The expected value of  $\hat{\sigma}_g$  (estimated using Eq. (3.11)) after reconstructing an image by averaging multiple acquisitions or by denoising is a value close to 27.5. Among the denoising methods considered, the estimated value of  $\hat{\sigma}_g$  more close to 27.5 is the one denoised with RLML. This experiment on the real data set additionally indicates that the image denoised with the proposed method is more close to the ground truth than other methods.

### 3.4 Conclusion

A new method to denoise MR images by applying the ML method locally to the restricted neighborhood is proposed in this chapter. A scheme is developed

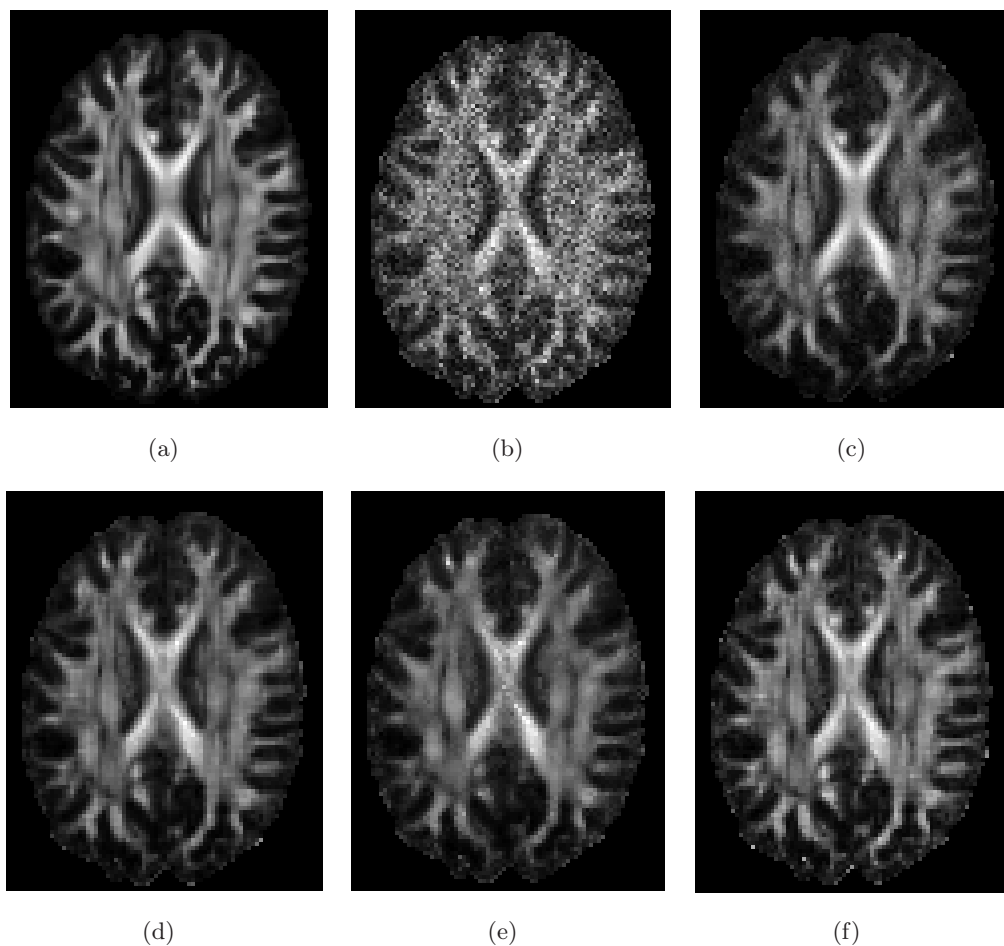


Figure 3.9: Experiments on the DWI atlas of the human brain (a) FA map computed from the ground truth (b) FA map computed after corrupting the original image with Rician noise of  $\sigma_g = 100$  (c) FA map computed from the image denoised with NLML method (d) FA map computed from the image denoised with UNLM method (e) FA map computed from the image denoised with RNRAD method (d) FA map computed from the image denoised with the proposed RLML method.

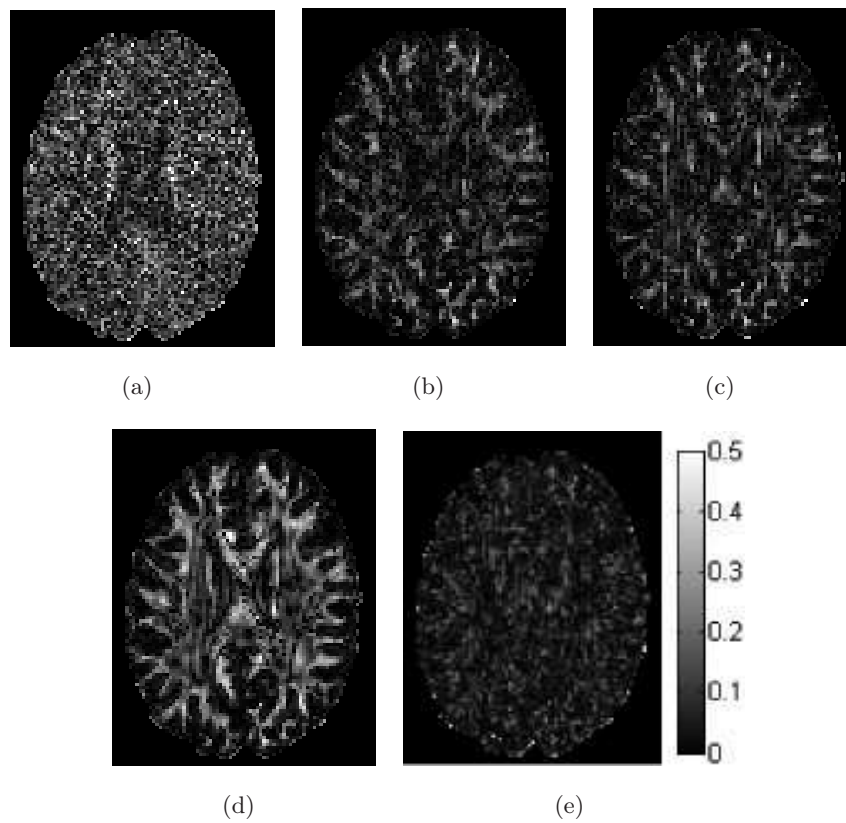


Figure 3.10: Absolute FA residuals (a) Noisy (MAD : 0.1189) (b) NLML method (MAD : 0.0560) (c) UNLM method (MAD : 0.0531) (d) RNRAD method (MAD : 0.0640) (e) proposed RLML method (MAD : 0.0505).

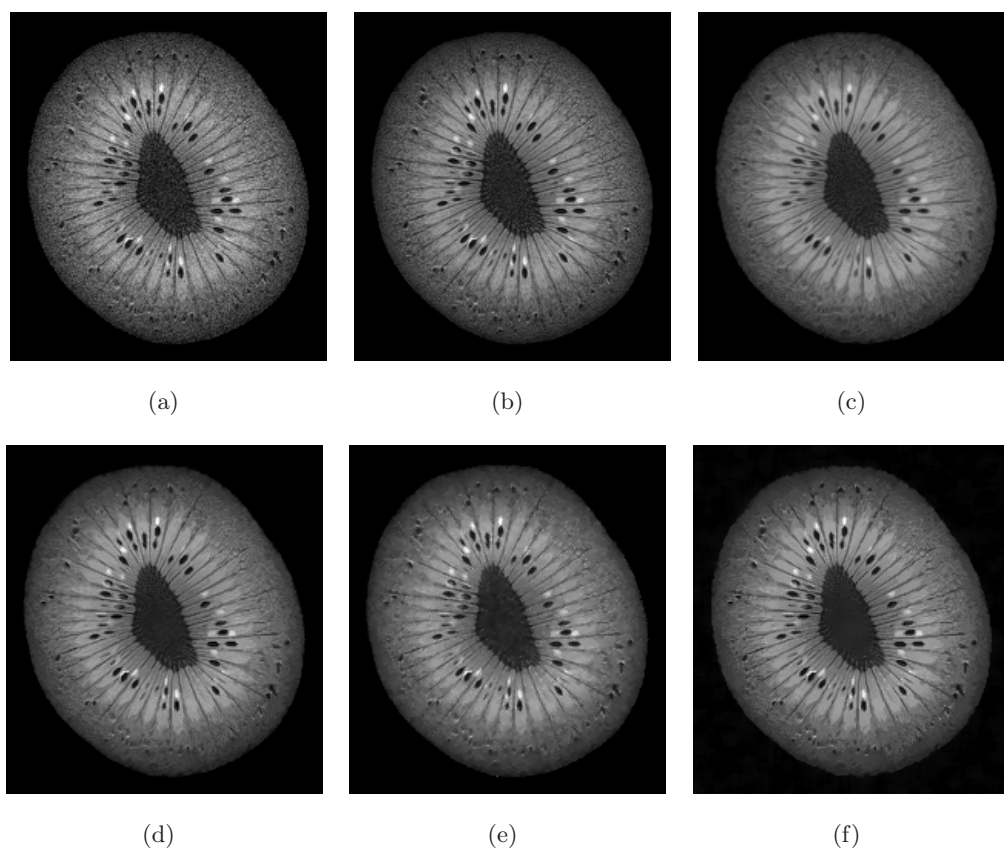


Figure 3.11: Experiments on the MR image of a Kiwi fruit **(a)** Original image reconstructed with 1 average **(b)** Original image reconstructed with 12 averages **(c)** (a) denoised with NLML method (sample size :18) **(d)** (a) denoised with UNLM method **(e)** (a) denoised with RNRAD method **(f)** (a) denoised with RLML method.

Table 3.1: Quantitative analysis of the proposed method with other recently proposed methods based on Eq. (3.11). This experiment was conducted on the MR image of a kiwi fruit.

Method	Estimated $\hat{\sigma}_g$ based on Eq. (3.11)
Kiwi fruit with 1 average (noise standard deviation = 27.5)	
Kiwi fruit with 12 averages	31.01
NLML	32.84
UNLM	38.17
RNRAD	23.75
RLML	<b>30.18</b>

to locally select the appropriate subset of pixels from the neighborhood of each pixel. Through this approach the side effects of LML method, the blurring effect and the distortion of fine structures, can be reduced. Experiments have been carried out on simulated and real data sets. Quantitative analysis at various noise levels based on the similarity measures, PSNR, SSIM, BC and MAD shows that the proposed method is more effective than other state-of-the-art methods. Experiments were also performed on DW images to prove the efficacy of the proposed method. Mean absolute difference of the FA residuals shows that the image denoised with the proposed method is more close to the ground truth.

## References

- [1] W. A. Edelstein, P. A. Bottomley, and L. M. Pfeifer, “A signal-to-noise calibration procedure for NMR imaging systems,” *Med Phys*, vol. 11, no. 2, pp. 180–185, 1984.
- [2] R. M. Henkelman, “Measurement of signal intensities in the presence of noise in MR images,” *Med Phys*, vol. 12, no. 2, pp. 232–233, 1985.

- [3] E. R. McVeigh, R. M. Henkelman, and M. J. Bronskil, "Noise and filtration in magnetic resonance imaging," *Med Phys*, vol. 12, no. 5, pp. 586–591, 1985.
- [4] M. A. Bernstein, D. M. Thomasson, and W. H. Perman, "Improved detectability in low signal-to-noise ratio magnetic resonance images by means of phase-corrected real construction," *Med Phys*, vol. 16, no. 5, pp. 813–817, 1989.
- [5] H. Gudbjartsson and S. Patz, "The Rician distribution of noisy MRI data," *Magn Reson Med*, vol. 34, pp. 910–914, 1995.
- [6] A. Macovski, "Noise in MRI," *Magn Reson Med*, vol. 36, pp. 494–497, 1996.
- [7] D.K. Jones and P.J. Basser, "Squashing peanuts and smashing pumpkins": How noise distorts diffusion MR data," *Magnetic Resonance in Medicine*, vol. 52, pp. 979–993, 2004.
- [8] S. Aja-Fernández, G. Vegas-Sánchez-Ferrero, and A. Tristán-Vega, "About the background distribution in MR data: a local variance study," *Magn Reson Imaging*, vol. 28, pp. 739–752, 2010.
- [9] José V. Manjón, José Carbonell-Caballero, Juan J. Lull, Garcían García-Martí, Luís Martí-Bonmatí, and Montserrat Robles, "MRI denoising using non local means," *Medical Image Analysis*, vol. 12, pp. 514–523, 2008.
- [10] G. Gerig, O. Kubler, R. Kikinis, and F. A. Jolesz, "Nonlinear anisotropic filtering of MRI data," *IEEE Trans. Med. Imag.*, vol. 11, no. 2, pp. 221–232, 1992.
- [11] S. Aja-Fernández, C. Alberola-López, and C.F. Westin, "Noise and signal estimation in magnitude MRI and rician distributed images:a LMMSE approach," *IEEE Trans Imag Proc*, vol. 17, pp. 1383–1398, 2008.

- [12] J. Sijbers, A. J. den Dekker, A. Van der Linden, M. Verhoye, and D. Van Dyck, “Adaptive anisotropic noise filtering for magnitude MR data,” *Magn Reson Imaging*, vol. 17, no. 10, pp. 1533–1539, 1999.
- [13] A. A. Samsonov and C.R. Johnson, “Noise adaptive nonlinear diffusion filtering of mr images with spatially varying noise levels,” *Magn Reson Med*, vol. 52, pp. 798–806, 2004.
- [14] P. Perona and J. Malik, “Scale space and edge detection using anisotropic diffusion,” *IEEE Trans. Pattern Anal. Machine Intell.*, vol. 12, no. 7, pp. 629–639, 1990.
- [15] Y.L You and M. Kaveh, “Fourth order partial differential equations for noise removal,” *IEEE Trans Imag Proc*, vol. 9, no. 10, pp. 1723–1730, 2000.
- [16] Marius Lysaker, Arvid Lundervold, and Xue-Cheng Tai, “Noise removal using fourth-order partial differential equation with applications to medical magnetic resonance images in space and time,” *IEEE Trans Imag Proc*, vol. 12, no. 12, pp. 1579–1590, 2003.
- [17] S. Basu, T. Fletcher, and R. Whitaker, “Rician noise removal in diffusion tensor MRI,” in *Medical Image Computing and Computer-Assisted Intervention - MICCAI 2006*, Berlin, 2006, pp. 117–125, Springer-Verlag.
- [18] K. Krissian and S. Aja-Fernández, “Noise driven anisotropic diffusion filtering of MRI,” *IEEE Trans Imag Proc*, vol. 18, pp. 2265–2274, 2009.
- [19] R. D. Nowak, “Wavelet based Rician noise removal for magnetic resonance images,” *IEEE Trans. Image Processing*, vol. 10, no. 8, pp. 1408–1419, 1999.
- [20] J. C. Wood and K. M. Johnson, “Wavelet packet denoising of magnetic resonance images: Importance of Rician noise at low SNR,” *Magn Reson Med*, vol. 41, no. 3, pp. 631–635, 1999.

- [21] A. Pizurica, W. Philips, I. Lemahieu, and M. Acheroy, “A versatile wavelet domain filtration technique for medical imaging,” *IEEE Trans Med Imaging*, vol. 22, pp. 323–331, 2003.
- [22] W. C. K. Wong and A. C. S. Chung, “Trilateral filtering: a non linear noise reduction technique for mri,” in *Proceedings of the International Society of Magnetic Resonance in Medicine*, Kyoto, Japan, May 2004, p. 2218.
- [23] I. Delakis, O. Hammad, and R. I. Kitney, “Wavelet based denoising algorithm for images acquired with parallel magnetic resonance imaging (MRI),” *Phys Med Biol*, vol. 52, pp. 3741–3751, 2007.
- [24] A. Buades, B. Coll, and J. M. Morel, “A review of image denoising algorithms, with a new one,” *Multiscale Model Simul*, vol. 4, pp. 490–530, 2005.
- [25] P. Coupé, P. Yger, S. Prima, P. Hellier, and Barillot C C. Kervarann, “An optimized blockwise nonlocal means denoising filter for 3d magnetic resonance images,” *IEEE Trans Med Imaging*, vol. 27, pp. 425–441, 2008.
- [26] N. Wiest-Daesslé, S. Prima, P. Coupé, S.P. Morrissey, and C. Barillo, “Rician noise removal by non-local means filtering for low signal-to-noise ratio MRI: Applications to DT-MRI,” in *Medical Image Computing and Computer-Assisted Intervention - MICCAI 2008*, Berlin, 2008, pp. 171–179, Springer-Verlag.
- [27] S. Aja-Fernández and K. Krissian, “An unbiased non local means scheme for DWI filtering,” in *Medical Image Computing and Computer-Assisted Intervention - MICCAI 2008*, Berlin, 2008, pp. 1277–284, Springer-Verlag.
- [28] José V. Manjón, P. Coupé, Luis Martí-Bonmatíand, D. Louis Collins, and Montserrat Robles, “Adaptive non local means denoising of MR images with spatially varying noise levels,” *J Magn Reson Imaging*, vol. 31, pp. 192–203, 2010.

- [29] J. Sijbers and A. J. den Dekker, “Maximum likelihood estimation of signal amplitude and noise variance from MR data,” *Magn Reson Med*, vol. 51, no. 3, pp. 586–594, 2004.
- [30] L. He and I. R. Greenshields, “A nonlocal maximum likelihood estimation method for rician noise reduction in MR images,” *IEEE Trans Med Imaging*, vol. 28, pp. 165–172, 2009.
- [31] Cheng Guan Koay, E. Özarslan, and Peter J. Basser, “A signal transformational framework for breaking the noise floor and its applications in MRI,” *Journal of Magnetic Resonance*, vol. 197, pp. 108–119, 2009.
- [32] J. Rajan, D. Poot, J. Juntu, and J. Sijbers, “Noise measurement from magnitude MRI using local estimates of variance and skewness,” *Phys Med Biol*, vol. 55, pp. N441–N449, 2010.
- [33] P. Thunberg and P. Zetterberg, “Noise distribution in SENSE - and GRAPPA - reconstructed images: a computer simulation study,” *Magn Reson Imaging*, vol. 25, pp. 1089–1094, 2007.
- [34] C. A. Cocosco, V. Kollokian, R.K.-S. Kwan, and A. C. Evans, “Brainweb: Online interface to a 3D MRI simulated brain database; <http://www.bic.mni.mcgill.ca/brainweb/>,” *NeuroImage*, vol. 5, no. 4, pp. S425, 1997.
- [35] A. Leemans, J. Sijbers, M. Verhoye, A. Van der Linden, and D. Van Dyck, “Mathematical framework for simulating diffusion tensor mr neural fiber bundles,” *Magnetic resonance in medicine*, vol. 53, no. 4, pp. 944–953, 2005.
- [36] A. Leemans, B. Jeurissen, J. Sijbers, and DK. Jones, “Exploredti: a graphical toolbox for processing, analyzing, and visualizing diffusion MR data.,” in *ISMRM 17-th scientific meeting*, 2009, p. 3537.
- [37] Z. Wang, A.C. Bovik, H. R. Sheikh, and E. P. Simoncelli, “Image quality assessment: From error visibility to structural similarity,” *IEEE Trans. on Image Processing*, vol. 13, pp. 600–612, 2004.

- [38] A. Bhattacharyaa, “On the measure of divergence between two statistical populations defined by their probability distributions,” *Bull Calcutta Math Soc*, vol. 35, pp. 99–109, 1943.
- [39] Q. Chen, Q. Sun, and D. Xia, “Homogeneity similarity based image denoising,” *Pattern Recognition*, vol. 43, pp. 4089–4100, 2010.

# Estimation and removal of noise from multiple-coil MR images

---

## Contents

---

<b>4.1</b>	<b>Introduction</b>	68
<b>4.2</b>	<b>Theory</b>	69
<b>4.3</b>	<b>Methods</b>	70
4.3.1	Extended NLML Method	70
4.3.2	Estimation of the number of coils $L$	72
<b>4.4</b>	<b>Experiments and Results</b>	74
<b>4.5</b>	<b>Conclusion</b>	79

---

The work described in this chapter has been published as:

**J. Rajan**, J. Veraart, J. Van Audekerke, M. Verhoye and J. Sijbers, “Nonlocal maximum likelihood estimation method for denoising multiple-coil magnetic resonance images”, *Magnetic Resonance Imaging*, In Press, 2012 (available online)

## Abstract:

Estimation and removal of noise from MR images is important for proper analysis, accurate parameter estimation and for further preprocessing of these

images. Many methods have been proposed in the literature for MRI noise estimation and denoising. However, not many approaches were suggested for estimating noise level or underlying true signal from MR images acquired with multichannel surface-coil arrays. If the magnitude image from surface-coil arrays are reconstructed as the root sum of squares, in the absence of noise correlations and subsampling, the data is assumed to follow a non central- $\chi$  distribution. However, parallel imaging and reconstruction methods can influence the statistical distribution of the data. The subsampling of  $k$ -space makes the noise level in the image spatially varying. In this chapter we propose a method for estimating the noise level and underlying true signal from multiple-coil acquired MR images in which the data follows a non central- $\chi$  distribution. Experiments were conducted on both simulated and real data sets to validate and to demonstrate the effectiveness of the proposed method.

## 4.1 Introduction

Stochastic noise is one of the main causes of quality deterioration in MRI and, hence, estimation and removal of noise remains an active area of research. Consideration of how noise affects the true signal is important for proper interpretation and analysis of MR images [1]. As discussed in the previous chapters, it is usually assumed that the noise in the MRI  $k$ -space data from each receiver channel is normally distributed. Due to the orthogonality of the Fourier basis functions, the noise remains Gaussian distributed after an inverse Fourier transform. However, the subsequent nonlinear operation, being the computation of the root of the sum of squares (SoS) of the Gaussian distributed complex image(s), leads to a magnitude image, which is no longer Gaussian distributed. In single coil systems, such magnitude data is governed by a stationary Rician distribution. For multi-coil systems, the magnitude image is non central Chi (nc- $\chi$ ) distributed, provided that the  $k$  space is fully sampled and no correlations between the coil data exists [2, 3].

For multi-coil systems, the data distribution also depends on the reconstruction techniques used. Multiple coil systems were initially developed to enhance the SNR of the acquired images (the smaller the sensitive volume of

a coil, the lower the noise from the adjacent structures and better the SNR will be) and later pMRI techniques were employed to it to accelerate the acquisition process through  $k$ -space subsampling. The advantages of pMRI are numerous (for e.g. fast imaging, breath-hold scans, increased temporal resolution, reduction of certain artifacts etc). The main trade-off from using pMRI is that the SNR decreases by at least the square root of the acceleration factor and the noise displays inhomogeneous spatial distribution.

In the recent past, several adaptive filtering techniques to improve the quality of magnitude MR images have been proposed [4, 5, 6, 7, 8, 9]. The Rician nature of the noise was incorporated in most of these methods to make it a suitable candidate for denoising magnitude MR images. However, none of the aforementioned methods are adapted to deal with nc- $\chi$  distributed data. Employing a Rician model to describe nc- $\chi$  distributed data (if the number of coils  $> 1$ ) may, however, introduce a bias in the estimated parameters. This bias will increase with increasing number of coils. However, multi-channel MRI acquisition schemes with pMRI techniques are becoming increasingly popular. Very recently, Brion et al. [10] proposed a method to estimate the underlying true signal from nc- $\chi$  distributed data. In their paper, a Linear Minimum Mean Square Estimator (LMMSE) method was used to estimate the true underlying intensity. In this chapter, a recently proposed non local maximum likelihood (NLML) estimation method [11] is extended to deal with nc- $\chi$  distributed and the spatially varying nature of the noise, which significantly increases its applicability.

In section 4.2 and 4.3, the theory behind the denoising method is clarified. In section 4.4, results are shown on simulated as well as experimental MR images. Finally, conclusions are drawn in section 4.5.

## 4.2 Theory

In a multiple-coil MR acquisition system, the acquired signal in the presence of noise, in each coil can be typically modeled as a complex Gaussian process. Thus, the complex signal in each coil  $l$  (for  $l = 1, 2, \dots, L$ ) after the inverse

Fourier transform can be expressed as [3]

$$C_l(\mathbf{x}) = S_l(\mathbf{x}) + n_l(\mathbf{x}; \sigma_g^2) \quad (4.1)$$

where  $S_l(\mathbf{x})$  represents the true complex signal in the absence of noise for each coil  $l$  and  $n_l(\mathbf{x}; \sigma_g^2) = n_{l_r}(\mathbf{x}; \sigma_g^2) + jn_{l_i}(\mathbf{x}; \sigma_g^2)$ , the complex Gaussian noise in each coil  $l$ . If no subsampling is done, the composite magnitude signal  $M_L(\mathbf{x})$  can be written as [12, 3]

$$M_L(\mathbf{x}) = \sqrt{\sum_{l=1}^L |C_l(\mathbf{x})|^2} \quad (4.2)$$

Assuming absence of noise correlation and that the  $L$  coils are statistically independent, the probability density function (PDF) of the composite magnitude signal,  $M_L$ , follows a nc- $\chi$  distribution defined by:

$$p_{M_L}(m) = \frac{m^L}{\sigma_g^2} a^{1-L} e^{-\frac{m^2+a^2}{2\sigma_g^2}} I_{L-1} \left( \frac{ma}{\sigma_g^2} \right), m \geq 0 \quad (4.3)$$

where  $a$  is the underlying true composite magnitude signal in the absence of noise,  $\sigma_g^2$ , the variance of the Gaussian noise in the complex data which is assumed to be the same for all  $L$  channels and  $I_{L-1}$  is the  $(L-1)^{th}$  order modified Bessel function of the first kind.

## 4.3 Methods

The objective of the proposed method is to estimate the true underlying intensity  $a$  from the composite magnitude image in which the observations follow a nc- $\chi$  distribution. For this purpose, we extended the NLML method which was originally proposed for denoising images with Rician noise.

### 4.3.1 Extended NLML Method

Let  $m_1, m_2, \dots, m_n$  be  $n$  *i.i.d* nc- $\chi$  observations. Then the joint PDF of the observation is

$$p(\{m_i\}|a) = \prod_{i=1}^n \frac{m_i^L}{\sigma_g^2} a^{1-L} e^{-\frac{m_i^2+a^2}{2\sigma_g^2}} I_{L-1} \left( \frac{m_i a}{\sigma_g^2} \right) \quad (4.4)$$

Given the observed data and a model of interest, the unknown parameters in the PDF can be estimated by maximizing the corresponding likelihood function. The unknown parameter in Eq. (4.4) is the true underlying intensity  $a$ . However, if  $\sigma_g^2$  is not known in advance, it can also be estimated along with  $a$  by maximizing the likelihood function  $\mathcal{L}$  or equivalently  $\ln \mathcal{L}$ , with respect to  $a$  and  $\sigma_g^2$ :

$$\{\hat{a}_{ML}, \hat{\sigma}_{ML}^2\} = \arg\{\max_{a, \sigma_g^2}(\ln \mathcal{L})\} \quad (4.5)$$

where

$$\begin{aligned} \ln \mathcal{L} = & \sum_{i=1}^n \ln \left( \frac{m_i^L}{\sigma_g^2} \right) + n \ln (a^{1-L}) - \sum_{i=1}^n \frac{m_i^2 + a^2}{2\sigma_g^2} \\ & + \sum_{i=1}^n \ln I_{L-1} \left( \frac{m_i a}{\sigma_g^2} \right) \end{aligned} \quad (4.6)$$

and  $\hat{a}_{ML}$  and  $\hat{\sigma}_{ML}^2$  are the estimated underlying true intensity and the noise variance respectively. Nevertheless, to estimate  $\hat{a}_{ML}$  and  $\hat{\sigma}_{ML}^2$  for each pixel in the image using Eq. (4.5), samples  $\{m_i\}$  with identical underlying intensity and noise variance need to be selected. As mentioned in the previous chapter, the straightforward approach to select samples  $\{m_i\}$  is to select all pixels from a local neighborhood. However, it is clear that around edges and fine structures the assumption of uniform underlying intensity is violated, and, as a result, blurring will be introduced in the image. An alternate approach is to use non local (NL) pixels instead [11]. The NL pixels are selected based on the intensity similarity of the pixel neighborhood. If the neighborhoods of two pixels are similar, then their central pixels should have a similar meaning and thus similar gray values [13]. The similarity of the pixel neighborhoods can be computed by taking the intensity distance (Euclidian distance) between them [11]:

$$d_{i,j} = \|N_i - N_j\| \quad (4.7)$$

where  $d_{i,j}$  is the intensity distance between the neighborhoods  $N_i$  and  $N_j$  of the pixels  $i$  and  $j$ . For each pixel  $i$ , the intensity distance  $d$  between  $i$  and all other non local pixels  $j$  as defined by Eq. (4.7), in the search window are measured. The first  $k$  pixels are then selected as  $\{m_i\}$  after sorting the NL

pixels in the increasing order of the distance  $d$  for the maximum likelihood (ML) estimation. Even though, in theory the search window is the whole image, for complexity reasons most implementations restrict the search area to a window surrounding  $i$ . In our implementation, a search window of size  $11 \times 11 \times 11$  was used.

If the noise level is spatially invariant, the noise standard deviation,  $\sigma_g$ , can be estimated from the background region of the image. This  $\sigma_g$  can be used in Eq. (4.6) to estimate the underlying true intensity  $a$ . Estimating  $a$  using ML with a known  $\sigma_g$  converges faster and will be more precise than estimating both  $a$  and  $\sigma_g$  simultaneously. The noise level can be estimated from the background as:

$$\hat{\sigma}_g = \sqrt{\frac{2}{\pi} \frac{2^{L-1}(L-1)!}{(2L-1)!!} \langle M_B \rangle} \quad (4.8)$$

where  $\langle M_B \rangle$  is the mean of the central  $\chi$  distributed background region. An explicit segmentation is needed in this case to extract the background regions, which can be sometimes difficult. Also, artifacts (e.g. Ghost artifacts) can influence the estimation. Explicit segmentation, and to some extent, the influence of artifacts can be avoided by using the local statistics for noise estimation as suggested in [3] as:

$$\hat{\sigma}_g = \sqrt{\frac{2}{\pi} \frac{2^{L-1}(L-1)!}{(2L-1)!!} \text{mode}\{\langle M_B(i) \rangle\}} \quad (4.9)$$

where  $\langle M_B(i) \rangle$  corresponds to the local mean computed for each pixel  $i$  in the image.

### 4.3.2 Estimation of the number of coils $L$

An important parameter in the nc- $\chi$  pdf is the number of coils  $L$ . Usually the experimenter knows  $L$  in advance. However,  $L$  can also be computed from the data statistics. If the  $k$ -space is not subsampled and if the background pixels in the acquired magnitude image follow a central  $\chi$  distribution, then the number of coils can be estimated from the SNR of the background region (the ratio of the mean of the central  $\chi$  distributed background region and its

standard deviation). This SNR from the background region will be constant for a particular  $L$  [14, 2]. This can be easily proved from the moments of the central- $\chi$  distribution.

Let  $M_B$  represent the background region of the composite magnitude image. Then the first and second moments of  $M_B$  can be written as [12, 14]:

$$\langle M_B \rangle = \beta_L \sigma_g \quad (4.10)$$

and

$$\langle M_B^2 \rangle = 2L\sigma_g^2 \quad (4.11)$$

where

$$\beta_L = \sqrt{\frac{\pi}{2}} \frac{(2L-1)!!}{2^{L-1}(L-1)!} \quad (4.12)$$

The variance of  $M_B$  in terms of the moments can be written as:

$$\sigma_{M_B}^2 = \langle M_B^2 \rangle - \langle M_B \rangle^2 \quad (4.13)$$

Substituting Eq. (4.10) and Eq. (4.11) in Eq. (4.13) yields

$$\sigma_g = \frac{\sigma_{M_B}}{\sqrt{2L - \beta_L^2}} \quad (4.14)$$

Now by substituting Eq. (4.14) in Eq. (4.10) we can compute the SNR as:

$$\frac{\langle M_B \rangle}{\sigma_{M_B}} = \frac{\beta_L}{\sqrt{2L - \beta_L^2}} \quad (4.15)$$

This SNR will always be a constant for a particular value of  $L$  as long as the background follows a central- $\chi$  distribution. SNR for different values of  $L$  computed using Eq. (4.15) is given in Table. 4.1. In summary,  $L$  can be predicted by measuring the SNR of the background region of the image. However, when the  $k$ -space is subsampled or if there exists correlation between the data from different coils, then the background region will not strictly follow a central- $\chi$  distribution and as a result the values in Table. 4.1 may not hold. This is discussed in detail in the work of Aja-Fernández et al. [15].

Table 4.1: *SNR* of the central  $\chi$  distributed background region for different values of  $L$ 

$L$	1	2	4	8	16	32	64
<i>SNR</i>	1.9131	2.7548	3.9429	5.6146	7.9694	11.2918	15.9845

#### 4.4 Experiments and Results

Synthetic experiments for image denoising were carried out on the standard BrainWeb MR volume [16]. In the first experiment, a synthetic image was created by multiplying the BrainWeb image with eight complex-valued coil sensitivities. Gaussian noise was then added to the real and imaginary parts of the image from each coil before creating the final magnitude image using the SoS method. Due to the SoS operation, the noise in the magnitude image follows a  $nc$ - $\chi$  distribution. This noisy image is then denoised with the proposed method and also with the LMMSE method in [10], which was recently proposed for denoising  $nc$ - $\chi$  distributed MR images. The denoising methods were executed with the following parameters. (i) proposed method : search window size :  $11 \times 11 \times 11$ , neighborhood size :  $3 \times 3 \times 3$  and sample size  $k = 20$  (ii) LMMSE : window size:  $5 \times 5 \times 5$ . The noise variance  $\sigma_g^2$  used in both methods was estimated using Eq. (4.9).

The visual quality comparison of the methods can be made from the results given in Fig. 4.1. As mentioned earlier, in visual analysis, the expectations are (i) perceptually flat regions should be as smooth as possible (ii) image edges and corners should be well preserved (iii) texture detail should not be lost and (iv) few or ideally no artifacts [11, 17]. It can be observed from Fig. 4.1 that the image denoised with the proposed method is closer to the original one (based on the above mentioned criteria) than the image denoised with the LMMSE approach. This is clearly visible from the residual images. For quantitative analysis, the experiment was repeated with various values of  $\sigma_g$  varying from 5 to 30 and the results based on PSNR and mean SSIM [18] are given in the Table. 4.2. In the quantitative analysis, the background region was excluded; that is, only the area of the image inside the skull was considered. The values in Table. 4.2 highlight the effectiveness of

#### 4.4. Experiments and Results

Table 4.2: Quantitative analysis of the proposed method with LMMSE method proposed in [10]. This experiment was conducted on the synthetic image of the brain reconstructed with SoS method with  $L = 8$ .

$\sigma_g$	5	10	15	20	25	30
Noisy						
PSNR	35.23	28.15	23.29	19.73	16.87	14.48
MSSIM	0.9318	0.8129	0.6938	0.5978	0.5157	0.4466
LMMSE						
PSNR	<b>37.05</b>	32.42	30.12	28.95	28.11	27.45
MSSIM	0.9618	0.9131	0.8703	0.8407	0.8155	0.7882
Proposed						
PSNR	36.01	<b>35.38</b>	<b>34.01</b>	<b>32.27</b>	<b>30.45</b>	<b>28.71</b>
MSSIM	<b>0.9706</b>	<b>0.9612</b>	<b>0.9371</b>	<b>0.9021</b>	<b>0.8612</b>	<b>0.8118</b>

the proposed method for denoising nc- $\chi$  data.

In the second experiment, synthetic images were reconstructed with SoS, SENSE [19] and GRAPPA [20] method using 4 coils. For SENSE and GRAPPA an acceleration factor of 2 were used. Gaussian noise of standard deviation,  $\sigma_g = 10$ , was added to the complex synthetic image (4 complex images with different sensitivities) to create the noisy image. The SoS image was reconstructed from the complex images by taking the root sum of squares. For SENSE and GRAPPA reconstruction experiment, the complex  $k$ -space images were created by taking the Fourier transform of the complex noisy image. These  $k$ -space images were then subsampled with a factor of 2. SENSE and GRAPPA methods were then applied to reconstruct the images from the subsampled  $k$ -space images. The PULSAR toolbox [21] was used for the SENSE and GRAPPA reconstruction. The proposed denoising algorithm was then applied over all the 3 reconstructed magnitude images (i.e., SoS, SENSE and GRAPPA). In the case of denoising SENSE reconstructed images, the number of coils  $L$  should be taken as 1, since the final magnitude

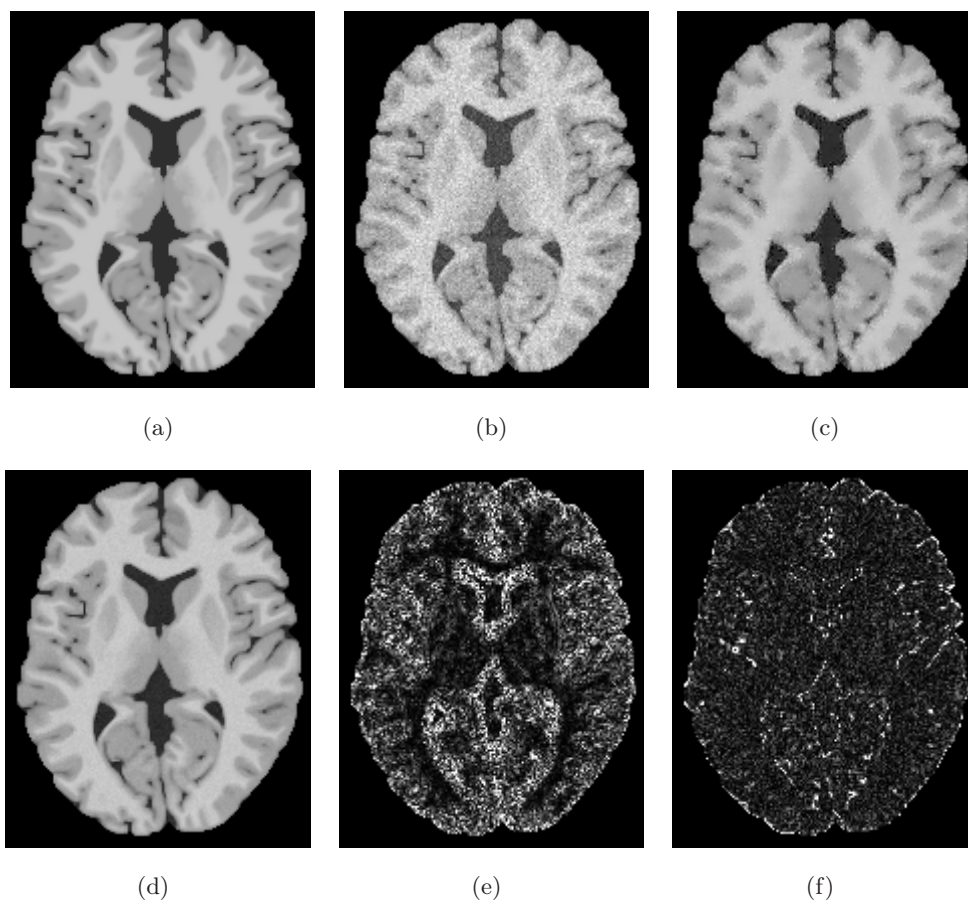


Figure 4.1: Denoising of MRI with  $nc\text{-}\chi$  distributed noise. (a) Ground Truth reconstructed with SoS method with  $L = 8$  (b) Ground Truth corrupted with  $nc\text{-}\chi$  distributed noise of  $\sigma_g = 15$  (c) denoised with LMMSE method (d) denoised with proposed method (e) and (f) corresponding residual images of (c) and (d) (scale 0-25).

images is generated from only 1 complex (composite) image. Hence in SENSE reconstructed images, the noise will be Rician distributed (which is a special case of nc- $\chi$  with  $L=1$ ), but spatially varying. The result of this experiment is shown in Fig. 4.2.

It can be observed from the results that the proposed method performs well in all the cases. However, there is some bias in the denoised image of the GRAPPA reconstructed image which is visible in the residual image. This bias is because of the influence of the signal correlation in  $L$ . The denoising experiment was executed with a constant value for  $L$  (in this case  $L=4$ ). Even if the coils are initially uncorrelated (which was the case in our simulations), signals will be correlated due to GRAPPA reconstruction [22]. The correlation will increase with the increase in the number of coils used for image acquisition. Correlations will affect the number of degrees of freedom of the distribution [15]. As a result, the value of the number of coils,  $L$ , will reduce and vary across the image. Ignoring effective  $L$  can thus create bias in the denoised image especially when there is high signal correlation. However, estimation of effective  $L$  requires raw MR data from each coil. Also, maximum likelihood estimation might not converge properly when the selected samples doesn't exactly follows the nc- $\chi$  distribution (especially when estimating  $A$  and  $\sigma$  simultaneously with a large  $L$ ).

For the experiments on the real data, we acquired ex vivo MR images (2D) of a mouse brain with a  $2 \times 2$  channel phased array coil using Bruker 7.0 T scanner. The images were acquired with SoS and GRAPPA (with an acceleration factor of 2) and later an image was also reconstructed with SENSE (with an acceleration factor of 2) from the raw data using the PULSAR tool box. The proposed denoising method was then applied on all the three reconstructed images. The results are shown in Fig. 4.3. This experiment on the real data set additionally indicates the effectiveness of the proposed method. We also analyzed the background region of the acquired SoS image to check whether there is any significant correlation between the data from different coils. If there is no significant correlation, the background region of the SoS image should follow a central- $\chi$  distribution. Fig. 4.4 shows the distribution of the background region of the mouse brain image acquired with

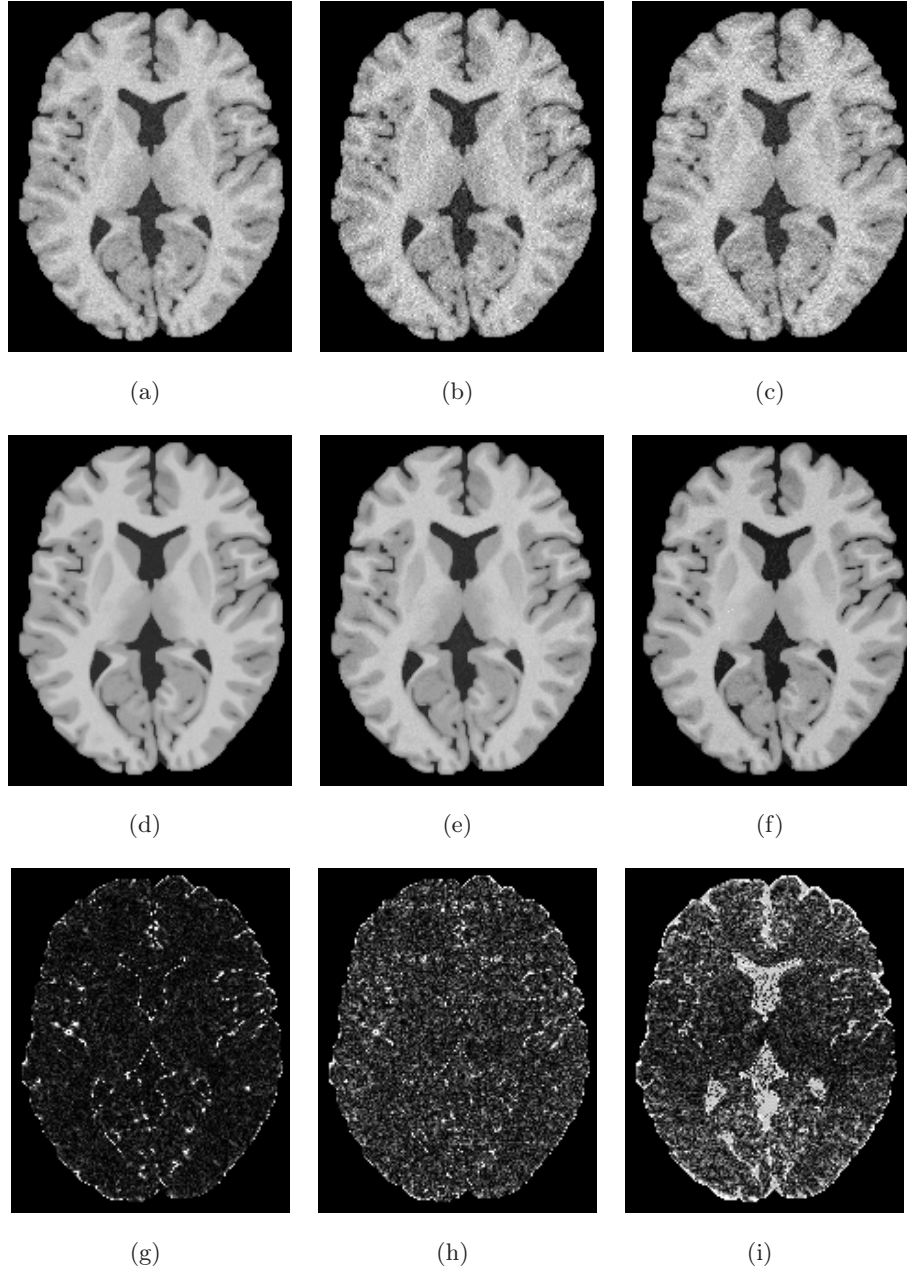


Figure 4.2: Denoising of multiple-coil acquired MRI. (a)[PSNR: 29.49,MSSIM: 0.8256], (b)[PSNR: 24.44,MSSIM: 0.6749] and (c)[PSNR: 24.77,MSSIM: 0.6848] are images acquired with  $L = 4$  and  $\sigma_g = 10$  and reconstructed with SoS, SENSE and GRAPPA (acceleration factor: 2) respectively. (d) [PSNR: 34.88, MSSIM: 0.9714], (e) [PSNR: 31.81, MSSIM: 0.9079] and (f) [PSNR: 28.41, MSSIM : 0.9111] are the denoised images of SoS, SENSE and GRAPPA reconstructed images. (g),(h) and (i) are the corresponding residual images (scale 0-25) with respect to the Ground Truth

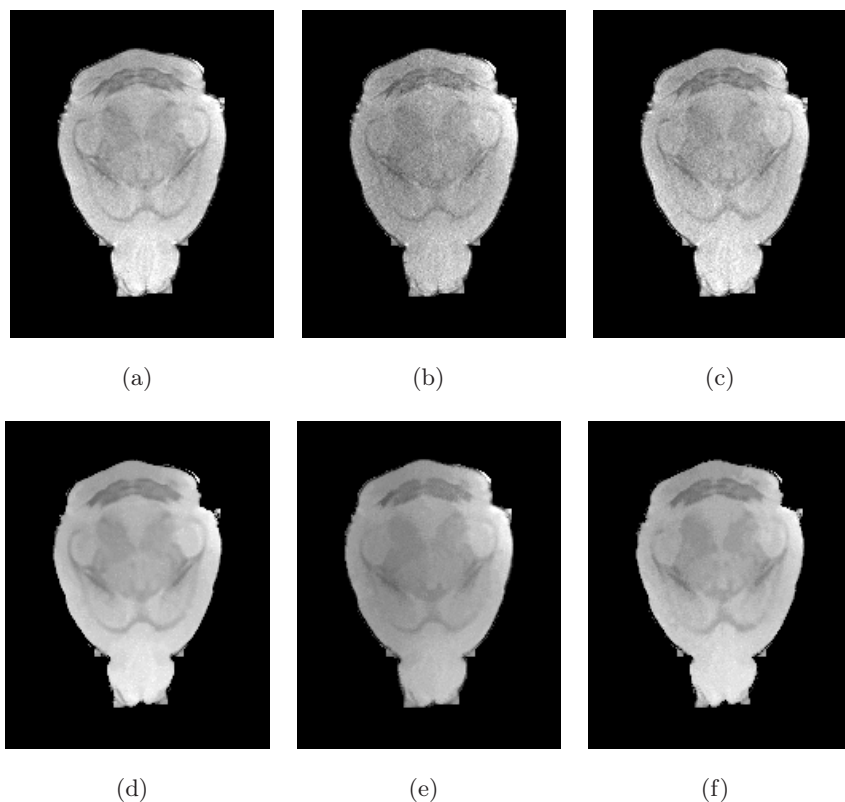


Figure 4.3: Experiments on ex vivo mice images. (a) (b) and (c) original mice image acquired with  $2 \times 2$  channel phased array coil and reconstructed with SoS, SENSE and GRAPPA. (d), (e) and (f) are the corresponding denoised images using the proposed method.

SoS method. Comparison with the true central- $\chi$  distribution shows that there is no significant correlation between the signals from different coils in this case.

## 4.5 Conclusion

We have proposed a method to denoise MR images in which the data follows a  $nc-\chi$  distribution. The proposed method is an extension of the NLML method which was proposed for denoising images corrupted with Rician noise. We extended this method to  $nc-\chi$  distributed data and also the spatially varying nature of the noise is incorporated. Experiments were conducted on both

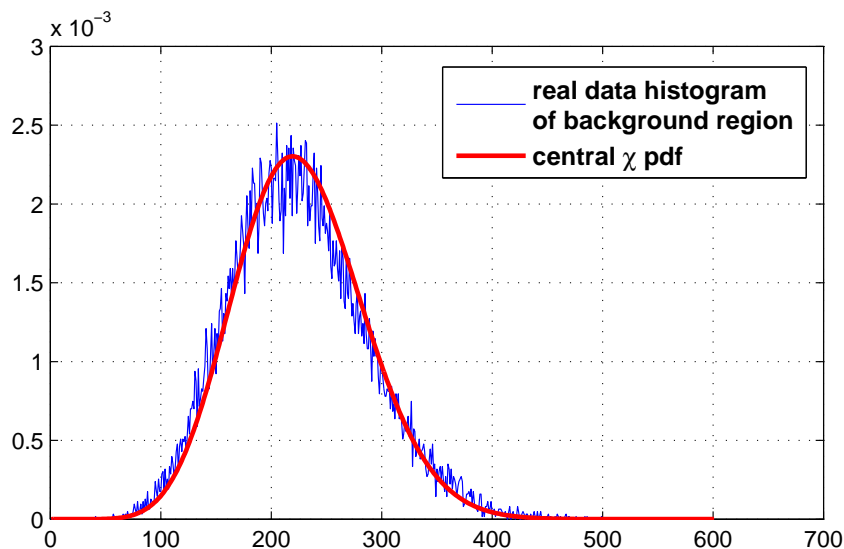


Figure 4.4: Actual distribution of the background region of the mice image (acquired with SoS with  $L = 4$ ) compared with the central- $\chi$  PDF (with  $L = 4$  and  $\sigma_g$  estimated from the background region of the image).

simulated and real images. The experimental results shows that the proposed method is very effective for MR images which follows nc- $\chi$  distribution.

## References

- [1] B A Landman, P L Bazin, and J L Prince, “Estimation and application of spatially variable noise fields in diffusion tensor imaging,” *Magnetic Resonance Imaging*, vol. 27, pp. 741–751, 2009.
- [2] O. Dietrich, J G Raya, S B Reeder, M Ingrisich, M F Reiser, and S O Schoenberg, “Influence of multichannel combination, parallel imaging and other reconstruction techniques on mri noise characteristics,” *Magnetic Resonance Imaging*, vol. 26, pp. 754–762, 2008.
- [3] S. Aja-Fernández, A. Tristán, and C. Alberola-López, “Noise estimation in single and multiple coil magnetic resonance data based on statistical models,” *Magn Reson Imaging*, vol. 27, pp. 1397–1409, 2009.

- [4] J. Sijbers, A. J. den Dekker, A. Van der Linden, M. Verhoye, and D. Van Dyck, “Adaptive anisotropic noise filtering for magnitude MR data,” *Magn Reson Imaging*, vol. 17, no. 10, pp. 1533–1539, 1999.
- [5] José V. Manjón, José Carbonell-Caballero, Juan J. Lull, Garcían García-Martí, Luís Martí-Bonmatí, and Montserrat Robles, “MRI denoising using non local means,” *Medical Image Analysis*, vol. 12, pp. 514–523, 2008.
- [6] K. Krissian and S. Aja-Fernández, “Noise driven anisotropic diffusion filtering of MRI,” *IEEE Trans Imag Proc*, vol. 18, pp. 2265–2274, 2009.
- [7] José V. Manjón, P. Coupé, Luis Martí-Bonmatíand, D. Louis Collins, and Montserrat Robles, “Adaptive non local means denoising of MR images with spatially varying noise levels,” *J Magn Reson Imaging*, vol. 31, pp. 192–203, 2010.
- [8] Jeny Rajan, Ben Jeurissen, Marleen Verhoye, Johan Van Audekerke, and Jan Sijbers, “Maximum likelihood estimation-based denoising of magnetic resonance images using restricted local neighborhoods,” *Physics in Medicine and Biology*, vol. 56, pp. 5221–5234, 2011.
- [9] Jeny Rajan, Johan Van Audekerke, Annemie Van der Linden, Marleen Verhoye, , and Jan Sijbers, “An adaptive non local maximum likelihood estimation method for denoising magnetic resonance images,” in *International Symposium on Biomedical Imaging*, 2012.
- [10] V. Brion, C. Poupon, O. Riff, S. Aja-Fernández, A. Tristán-Vega, J F Mangin, D L Bihan, and F. Poupon, “Parallel MRI noise correction : An extension of LMMSE to non central  $\chi$  distributions,” in *Medical Image Computing and Computer-Assisted Intervention - MICCAI 2011*, Berlin, 2011, pp. 226–233, Springer-Verlag.
- [11] L. He and I. R. Greenshields, “A nonlocal maximum likelihood estimation method for rician noise reduction in MR images,” *IEEE Trans Med Imaging*, vol. 28, pp. 165–172, 2009.

- [12] C. D. Constantinides, E. Atalar, and E. R. McVeigh, “Signal-to-noise measurements in magnitude images from NMR phased arrays,” *Magn Reson Med*, vol. 38, pp. 852–857, 1997.
- [13] S. Zimmer, S. Didas, and J. Weickert, “A rotationally invariant block matching strategy improving image denoising with non-local means,” in *International Workshop on Local and Non-Local Approximation in Image Processing*, Switzerland, 2008, pp. 135–142.
- [14] C G Koay and P J Basser, “Analytically exact correction scheme for signal extraction from noisy magnitude MR signals,” *Journal of Magnetic Resonance*, vol. 179, pp. 317–322, 2006.
- [15] S. Aja-Fernández and A. Tristán-Vega, “Influence of noise correlation in multiple-coil statistical models with sum of squares reconstruction,” *Magn Reson Med*, vol. 67, pp. 580–585, 2011.
- [16] C. A. Cocosco, V. Kollokian, R.K.-S. Kwan, and A. C. Evans, “Brainweb: Online interface to a 3D MRI simulated brain database; <http://www.bic.mni.mcgill.ca/brainweb/>,” *NeuroImage*, vol. 5, no. 4, pp. S425, 1997.
- [17] Q. Chen, Q. Sun, and D. Xia, “Homogeneity similarity based image denoising,” *Pattern Recognition*, vol. 43, pp. 4089–4100, 2010.
- [18] Z. Wang, A.C. Bovik, H. R. Sheikh, and E. P. Simoncelli, “Image quality assessment: From error visibility to structural similarity,” *IEEE Trans. on Image Processing*, vol. 13, pp. 600–612, 2004.
- [19] K. P. Pruessmann, M. Weiger, M. B. Scheidegger, and P. Boesiger, “SENSE : Sensitivity encoding for fast MRI,” *Magn Reson Med*, vol. 42, pp. 952–962, 1999.
- [20] M. A. Griswold, P. M. Jacob, R.M. Heidemann, M. Nittka, V. Wang, B. Kiefer, and A. Haase, “Generalized autocalibrating partially parallel acquisitions GRAPPA,” *Magn Reson Med*, vol. 47, pp. 1202–1210, 2002.

- [21] J. X. Ji, J. B. Son, and S. D. Rane, “PULSAR: A matlab toolbox for parallel magnetic resonance imaging using array coils and multiple channel receivers,” *Concepts in magnetic resonance part B : Magnetic Resonance Engineering*, vol. 31B(1), pp. 24–36, 2007.
- [22] S. Aja-Fernández, A. Tristán-Vega, and W S Hoge, “Statistical noise analysis in GRAPPA using a parametrized noncentral chi approximation model,” *Magn Reson Med*, vol. 65, pp. 1195–1206, 2011.



# Conclusions

The objective of this thesis was to develop effective methods for the estimation and removal of noise from MR images acquired with both single and multiple coils. MR images are always corrupted with noise and the SNR of the image is influenced by several factors like the strength of the main magnetic field, pulse sequence design, tissue characteristics, RF coil used and imaging parameters like voxel size, number of excitations, receiver bandwidth etc. Noise estimation and denoising plays an important role in the further processing of these images. Several methods were proposed in the literature for the estimation of the noise from magnitude MR images. However one drawback of most of those methods were their dependency on the Rayleigh distributed background region. New object based methods were introduced in this thesis to overcome those limitations.

For the denoising of MR images corrupted with Rician noise, we proposed a restricted local ML estimation method. Instead of selecting all the pixels in the local neighborhood region, the proposed RLML method selects only the pixels that is believed to have an underlying intensity close to that of the center pixel in the local window for the ML estimation of the true underlying intensity. Through putting restrictions on the pixel selection and thus by reducing the model violations, the proposed method preserves the fine structures in the image and also reduce the blurring effects which is common with local ML approach. Comparisons with the state-of-the art methods for denoising shows that the proposed method is more effective in terms of the quality matrices used for quantitative analysis and also based on the visual analysis. However there are still room to improve the proposed method. One drawback of the proposed method is its dependency on the reference image. It might be possible to use some statistical approaches for suitable sample selection from local neighborhood to avoid the dependency of the proposed method on a reference image. Further research is needed in this direction. Another area for improvement is in the threshold calculation. At

present a global threshold is used for pixel classification. A local threshold value can further improve the performance of the proposed method.

A generalized non local ML estimation method for noise estimation and denoising of MR images acquired with multiple coils is proposed in the last chapter. When more than one coil is used for image acquisition and if the magnitude images are created using the SoS method, then magnitude data generally follows a  $nc\text{-}\chi$  distribution. However, parallel imaging and reconstruction methods can influence the statistical distribution of the data. The subsampling of  $k$ -space for reducing the acquisition time makes the noise level in the image spatially varying. Both the  $nc\text{-}\chi$  distribution and spatially varying nature of the noise is taken into account in the proposed method. In the non local ML method, the samples for ML estimation is selected in a non local fashion based of the intensity similarity of the pixel neighborhood. This non local way of selecting the samples help in finding the similar pixels (with the same underlying intensity). This method is highly efficient when compared to local ML estimation. However one little concern in the non local ML estimation method is regarding the number of samples to be selected for ML estimation. In our implementations, this is fixed and generally determined in a heuristic way. An adaptive way of selecting the samples can further improve the results.

# List of Publications

List of publications(during my stay at the Vision Lab, 30 March 2009 - Till date).

## Journals

1. Jelle Veraart, **Jeny Rajan**, Ronald R. Peeters, Alexander Leemans, Stefan Sunaert, Jan Sijbers, "A comprehensive framework for estimating model parameters from real world diffusion MRI data", *Magnetic Resonance in Medicine*, In Press.
2. **Jeny Rajan**, Jelle Veraart, Johan Van Audekerke, Marleen Verhoye and Jan Sijbers, " Nonlocal maximum likelihood estimation method for denoising multiple-coil magnetic resonance images", *Magnetic Resonance Imaging* , In Press.
3. Riji R, **Jeny Rajan**, Jan Sijbers, Madhu S Nair, "MRI denoising using iterative bilateral filter", *Biomedical Signal Processing and Control* , In Review.
4. **Jeny Rajan**, Jelle Veraart, Jan Sijbers, "Object based noise estimation methods for MRI - A short review", In Progress.
5. Mai Zhenhua, **Jeny Rajan**, Marleen Verhoye, Jan Sijbers, " Robust edge-directed interpolation of magnetic resonance images". *Physics in Medicine and Biology*, vol. 56, pp. 7287-7303, 2011.
6. **Jeny Rajan**, Ben Jeurissen, Marleen Verhoye, Johan Van Audekerke and Jan Sijbers, " Maximum likelihood estimation based denoising of magnetic resonance images using restricted local neighborhoods", *Physics in Medicine and Biology*, Vol 56, pp 5221- 5234,2011.

7. **Jeny Rajan**, Dirk Poot, Jaber Juntu and Jan Sijbers, "Noise Measurement from magnitude MRI using local estimates of variance and skewness", *Physics in Medicine and Biology*, Vol 55, pp N441-N449, 2010.
8. Jaber Juntu, Jan Sijbers, Steve De Backer, **Jeny Rajan**, Dirk Van Dyck, "A machine learning study of several classifiers trained with texture analysis features to differentiate benign from malignant soft tissue tumors in T1-MRI images", *Journal of Magnetic Resonance Imaging*, Vol 31, pp 680-689, 2010.

### Conferences (published in proceedings)

1. **Jeny Rajan**, Johan Van Audekerke, Annemie Van der Linden, Marleen Verhoye and Jan Sijbers, "An adaptive non local maximum likelihood estimation method for denoising magnetic resonance images", *9<sup>th</sup> IEEE International Symposium on Biomedical Imaging (ISBI 2012)*, pp 1136-1139, 2012.
2. **Jeny Rajan**, Marleen Verhoye, Jan Sijbers, "A maximum likelihood estimation method for denoising magnitude MRI using restricted local neighborhood", *SPIE Medical Imaging 2011*, Vol. 7962,79624U, 2011.
3. **Jeny Rajan**, Jan Sijbers, Dirk Poot, Jaber Juntu, "Segmentation based noise variance estimation from background MRI data", *International Conference on Image Analysis and Recognition (ICIAR) 2010, (LNCS Vol. 6111)*, pp 62-70, 2010.
4. **Jeny Rajan**, Ben Jeurissen, Jan Sijbers, Kannan, "Denoising magnetic resonance images using 4<sup>th</sup> order complex diffusion", *13<sup>th</sup> International Machine Vision and Image Processing Conference (IMVIP)*, pp 123-127, 2009.

## Abstracts

1. Jelle Veraart, **Jeny Rajan**, Ronald R. Peeters, Alexander Leemans, Stefan Sunaert, Jan Sijbers, "Diffusion MRI: Estimation of spatially variable Rician noise", *29<sup>th</sup> Annual Scientific Meeting, European Society for Magnetic Resonance in Medicine and Biology (ESMRMB 2012)*, pp :266, 2012.
2. **Jeny Rajan**, Johan Van Audekerke, Jelle Veraart , Marleen Verhoye, Jan Sijbers, "An extended NLML method for denoising non-central chi distributed data - application to parallel MRI", *Fourth Annual Meeting of Benelux ISMRM Chapter*, pp 41, 2012.
3. **Jeny Rajan**, Jan Sijbers, "Denoising SENSE reconstructed MR images", *5<sup>th</sup> Annual Symposium of the Benelux Chapter of the IEEE Engineering in Medicine and Biology Society (EMBS)*, 2011.
4. Mai Zhenhua, **Jeny Rajan**, Marleen Verhoye, Jan Sijbers, "Robust edge directed interpolation of diffusion weighted MR images", *28<sup>th</sup> Annual Scientific Meeting, European Society for Magnetic Resonance in Medicine and Biology (ESMRMB 2011)*, Vol 4, pp :382, 2011.
5. **Jeny Rajan**, Johan Van Audekerke, Marleen Verhoye, Annemie Van der Linden and Jan Sijbers, "Denoising magnitude MRI using an adaptive NLML method", *28<sup>th</sup> Annual Scientific Meeting, European Society for Magnetic Resonance in Medicine and Biology (ESMRMB 2011)*, Vol 4, pp: 383, 2011
6. Maryna Kudiznova, **Jeny Rajan**, Jan Sijbers, " Denoising of DKI images: effect on feasibility and accuracy of kurtosis parameters", *28<sup>th</sup> Annual Scientific Meeting, European Society for Magnetic Resonance in Medicine and Biology(ESMRMB 2011)*, Vol 3, pp :236, 2011

